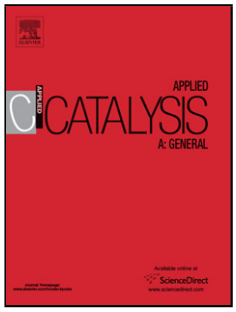

Title: Probing properties of the interfacial perimeter sites in $TiO_x/Au/SiO_2$ with 2-Propanol decomposition

Authors: Yi Y. Wu, Harold H. Kung

PII: S0926-860X(17)30276-4
DOI: http://dx.doi.org/doi:10.1016/j.apcata.2017.06.027
Reference: APCATA 16289

To appear in: *Applied Catalysis A: General*

Received date: 17-4-2017
Revised date: 19-6-2017
Accepted date: 21-6-2017

Please cite this article as: Yi Y.Wu, Harold H.Kung, Probing properties of the interfacial perimeter sites in TiOx/Au/SiO2 with 2-Propanol decomposition, Applied Catalysis A, Generalhttp://dx.doi.org/10.1016/j.apcata.2017.06.027

Probing Properties of the Interfacial Perimeter Sites in $TiO_x/Au/SiO_2$ with 2-Propanol Decomposition

Yi Y. Wu and Harold H. Kung*

Department of Chemical and Biological Engineering, Northwestern University, Evanston IL, 60208, USA

Graphical abstract

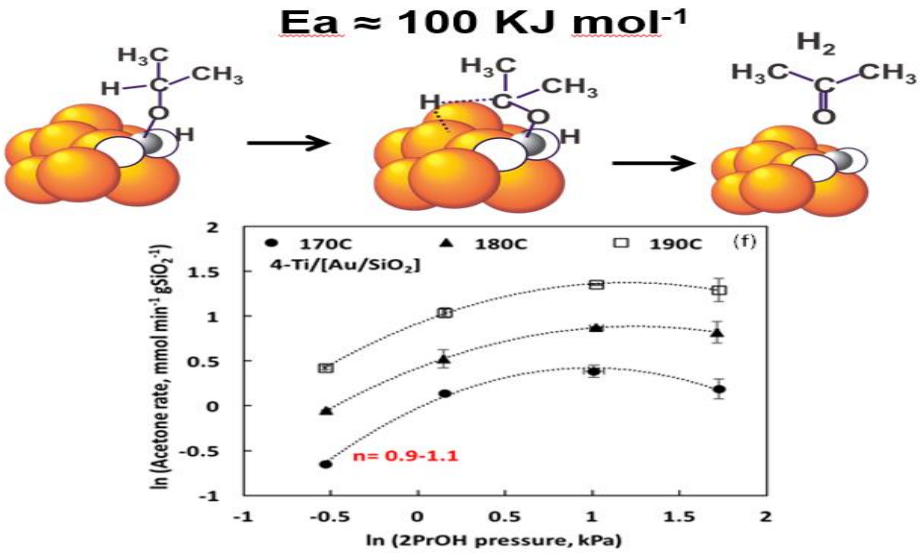

Highlights:

- Interfacial perimeter sites of Au with TiO_2 catalyze decomposition of 2-propanol to acetone selectively.
- Interfacial perimeter sites of Au with TiO_2 are much more active than Au surface.

Abstract

The decomposition of 2-propanol was studied over SiO_2, SiO_2 with an overlayer of TiO_2 (Ti/SiO_2), Au/SiO_2, and Au/SiO_2 with an overlayer of TiO_2 ($Ti/[Au/SiO_2]$) at 170-190 ºC. There was no reaction on SiO_2. Propene was the only product on Ti/SiO_2, and its rate of formation increased proportionally with the Ti content. Acetone was the major product (selectivity 65-99%) on all Au-containing catalysts. Its rate of formation also increased with Ti loading. In addition, small amounts of propene were also formed on $Ti/[Au/SiO_2]$ the rate of which increased with Ti loading. Characterization of the catalysts with N_2 adsorption, STEM, DR-UV-vis spectroscopy, XPS, XANES and EXAFS suggested that the Ti formed an amorphous TiO_2 overlayer on the catalyst. At high Ti loadings (4-5 wt.%), there were patches of thick porous TiO_2 layer, and some microdomains of crystalline TiO_2 could be detected. Au was present as 1 – 3 nm nanoparticles on all catalysts, before and after used in reaction. Only Lewis acid sites were detected based on results from pyridine adsorption, and their quantities increased with Ti loading. Based on the comparison of reaction rates, the dependence of the kinetics on 2-propanol partial

pressure, the apparent activation energies, and the effect of co-feeding O_2 among different catalysts, it was concluded that propene was formed on the TiO_2 overlayer, acetone was formed primarily at the Au-TiO_2 interfacial perimeter sites, and α-C-H bond breaking preceding acetone formation was more facile on Au at the interfacial site than other surface Au atoms. Implication of these results to the selective acetone formation in the oxidation of propane in the presence of a O_2/H_2 mixture was discussed.

Keywords: catalysis, 2-propanol decomposition, supported Au

1. Introduction

It has been demonstrated that Au is an effective catalysts for various selective oxidation reactions, such as benzyl alcohol oxidation [1], selective oxidation of styrene [2] and epoxidation of propene and butene [3-5]. It is particularly interesting that supported Au catalysts can produce acetone selectively from propane by oxidation with O_2 and H_2 [6-8]. This was first reported by Oyama and coworkers that acetone was formed with 84% selectivity using a Au/TS-1 catalyst, whereas propene was the selective product (69% selectivity) over Au/TiO_2 [8]. However, the very low conversions achieved substantially limited its commercial viability as a route for acetone production. In order to improve the production, it is useful to identify the active site and understand the reaction mechanism. Thus, subsequent to Oyama's report, we demonstrated that the interfacial perimeter site of Au with (Ti,Si)O_2 was essential for acetone formation [9, 10]. We showed that: (i) the reaction was much slower on Au/SiO_2 without these interfacial perimeter sites; (ii) the formation of acetone was faster with a higher density of these sites, and (iii) close proximity of (Ti,Si)O_2 to Au was necessary for rate enhancement.

The fact that Au/SiO_2 was much less active than catalysts with Au-(Ti,Si)O_2 interfacial perimeter sites implies that either activation of oxygen on these sites is much faster than on a Au surface or the oxygen species that is catalytically active is formed preferentially at these interfacial perimeter sites. An example of the latter would be an adsorbed hydroperoxy. Other than these, however, there is little mechanistic information on how these sites participate in the formation of acetone. In a mechanism proposed by Oyama [6], propane is activated by a surface hydroperoxy group to form an adsorbed 2-propoxy, which can undergo either α-C-H elimination to form acetone, or dehydration to form propene. Since dehydration of 2-propanol to form propene occurs readily on TiO_2 [11, 12], an interfacial perimeter site is not necessary for dehydration. On the other hand, only small amounts of acetone have been detected on TiO_2 both in steady state [11, 12] and temperature programmed reaction experiments [13-16]. This suggests participation of Au in its formation. One possibility is that at the interfacial perimeter sites, 2-propoxy is adsorbed on Ti, and Au is responsible for cleaving the α-C-H bond. If this is correct, we expect that these interfacial sites will also be very efficient in 2-propanol decomposition to form acetone. Indeed, there is evidence that Au-oxide interfacial perimeter sites are capable of acetone formation. In TPD of adsorbed 2-propanol, acetone was detected from Au/TiO_2 powder or a Au(111) surface with deposited nano-TiO_2 crystallites, while none was detected from TiO_2 powder [17] or a single crystal TiO_2 surface [18]. Likewise, adsorbed acetone derived from 2-propanol was observed by IR on Au/Al_2O_3 but not on Al_2O_3 [19].

The objective of this work is to investigate the decomposition of 2-propanol on TiO_x-modified Au/SiO_2, with a focus on generating information on the reaction of 2-propoxy at the

Au-TiO_x interfacial perimeter sites. In particular, reaction kinetics of product formation from 2-propanol decomposition was determined from which contributions from different sites on the catalysts were derived. Effect of oxygen in the feed was also investigated in order to relate these data to the selective formation of acetone in the oxidation of propane.

2. Experimental

2.1 Catalyst preparation

Au/SiO_2

The gold precursor, $Au(en)_2Cl_3$, was prepared with a procedure modified from [20]. $HAuCl_4 \cdot 3H_2O$ (1 g, > 99.9%, Sigma Aldrich) was dissolved in 4 mL of deionized (DI) water followed by addition of 20 mL ethanol (KOPTEC, 200 proof). After the solution was fully mixed, ethylenediamine (0.48 mL, ≥ 99%, ReagentPlus®, Sigma Aldrich) was added and a pale yellow precipitate was formed. The mixture was stirred for 10 minutes and then filtered and washed with 3 portions of 100 mL ethanol. The resulting pale yellow precipitate with a yield of ~1 g was stored in a freezer after drying under vacuum for 30 min.

Au/SiO_2 was prepared by a modified cationic deposition method [21]. Typically, $Au(en)_2Cl_3$ was dissolved in 40 °C DI water to obtain a 3.3-4.4 mM Au solution. After SiO_2 (nonporous, fumed Cab-O-Sil L90) was added to the gold solution with stirring, the heat was turned off. An aqueous 0.75 M ethylenediamine solution was added dropwise to the mixture to gradually adjust the PH to 9.0. After stirring the mixture at room temperature for 2 h, the Au/SiO_2 was filtered and washed with 500 mL room temperature DI water. The solid was redispersed in 40 °C DI water (100 mL DI water/g SiO_2) and stirred for 10 min. The mixture was filtered and washed again with 500 mL of DI water at room temperature until the concentration of Cl^- ions in the filtrate was below 30 ppm as indicated with Quantab Chloride Titrators. No detectable Cl was observed by XPS.

TiO_x/SiO_2, $TiO_x/[Au/SiO_2]$, and Au/TiO_2

$Ti(OiPr)_2(acac)_2$ (75 wt.% in 2-propanol, Sigma Aldrich) in tetrahydrofuran (THF) was used to prepare TiO_x/SiO_2 (whence labeled Ti/SiO_2) and Au/SiO_2 with TiO_x overcoat (labeled $Ti/[Au/SiO_2]$) by impregnation onto SiO_2 and Au/SiO_2, respectively. An amount of $Ti(OiPr)_2(acac)_2$ that would yield approximately 1 wt.% Ti was used to prepare 1-Ti/SiO_2 and 1-$Ti/Au/SiO_2$, and 4 to 5 wt.% (in 3 batches of ~1 wt.% each) for 5-Ti/SiO_2 and 4-$Ti/Au/SiO_2$. Assuming that the SiOH density was 5 SiOH/nm^2 [22] and that each 2-propoxy on $Ti(OiPr)_2(acac)_2$ would react with one SiOH on the surface, 1.5 wt.% Ti would roughly form one monolayer equivalent of TiO_x on the SiO_2.

Au/TiO_2 was prepared by deposition-precipitation. A 1.5 mM DI water solution of $HAuCl_4 \cdot 3H_2O$ was adjusted to pH 8.4 with 1 M NaOH solution. Then 3 g TiO_2 (anatase, 99.8%, ≤ 25 nm, 45-55 m^2/g, Sigma Aldrich) was dispersed in the gold solution. The resulting pH value was 6.94. The suspension was filtered, washed with 600 mL DI water, and the solid was calcined in air at 400 °C for 2 h and reduced in 5% H_2 at 150 °C for 1 h.

All the catalysts were treated with 10% ozone in O_2 at 300 mL/min and a thermal ramping rate of 0.12 °C min^{-1} to 150 °C to remove organic ligands before storage.

2.2 Catalytic reactions

The catalysts were pretreated with 100 mL min^{-1} 10% H_2 in He at 180 °C for 1 h to completely reduce Au nanoparticles prior to catalytic testing (Supporting Information Figure S2).

All reactions were conducted under atmospheric pressure in a quartz packed bed reactor. Any empty space in the reactor was filled with 10-16 mesh quartz chips to minimize gas-phase reactions.

Contact time was defined as the ratio of the catalyst weight to the total flow rate of 2-propanol (W/F_{2PrOH}), in the unit of (gCat. min mmol)$^{-1}$. Similar contact times were achieved by using different catalyst weights and/or adjusting the total flow rate of 2-propanol accordingly. Conversions increased linearly with increasing contact time, verifying that the reactions were carried out without external mass transfer limitation (Figure S3). The Weisz-Prater criteria was estimated to be 1.2×10^{-9}, implying that pore diffusion did not influence the kinetics (See Supplementary Information and Table S1). The gas phase products were analyzed online by gas chromatography-mass spectroscopy (Agilent 6890 GC-MSD 5973). The GC was equipped with a Porapak-Q (80-100 mesh) packed column with a thermal conductivity detector for analysis (O_2, CO_2, H_2O, propane, propene, acetone and 2-propanol), and the analysis was supplemented with a flame ionization detector and mass spectrometer coupled to a Agilent DB624 capillary column to detect propene, acetone and 2-propanol. No CO_2 formation was observed; conversion and selectivity are defined as follows:

Conversion
= moles of (C_3 products) / moles of (2-PrOH + C_3 products)
Selectivity of a C_3 product
= moles of a C_3 product/ total moles of all C_3 products

2-Propanol Decomposition

All catalysts were diluted with 4 times the weight of 40-80 mesh quartz chips, whereas 7 times the weight was used for TiO_2 and Au/TiO_2. 2-Propanol vapor was introduced via a flow of He through a saturator of anhydrous 2-propanol (99.5%, Sigma Aldrich). The saturator delivered a stream of at least 97% alcohol saturation [23]. The partial pressure of 2-PrOH were adjusted by changing the saturator temperatures (0 or 20-23 °C) and/or diluting with a stream of He. The range of 2-PrOH partial pressures tested was 0.6-5.6 kPa. Catalyst weight (25-200 mg) was adjusted depending on the catalyst activity to keep conversions less than 16% for kinetic studies. Kinetic data were collected at ~2 h time on stream when 2-propanol decomposition had reached a steady state (conversions at ~2 h and ~5 h differed by less than 10% of its value). Carbon balance was within 5% (see Table S1 for 4-Ti/[Au/SiO_2] as an example).

Propanol Oxidation with O_2

2-propanol vapor (99.5% anhydrous, Sigma Aldrich) was introduced via a flow of He in a saturator at 20-23 °C. The feed composition was 2-propanol/O_2/He=1.2/5/93.8 with a total flow rate of 30 mL min^{-1} at 180 °C. Catalytic data shown were the average values of data collected at 3-5 h time-on-stream when the reaction reached a steady state.

2.3 Characterization

Scintag XDS2000 diffractometer (Cu κα, 1.54 Å) was used to collect the XRD pattern of TS-1 (Figure S4). Scans started from 5° to 50° with a step size of 0.02° at a rate of 0.04 °/sec. The metal loadings were determined by Thermo iCAP 7600 ICP-OES. Samples were digested in small amounts of a mixture of concentrated hydrofluoric acid, nitric acid and hydrochloric acid before dilution to a metal concentration of about 4 ppm for analysis. Standards for Ti and Au

were prepared with 1000 ppm ICP standard solutions (Sigma Aldrich). The relative standard deviations (RSD) from replicate measurements for a sample were 0.9-2.6% for Au and 0.6-1.6% for Ti.

The BET surface areas, pore volumes and pore diameters were determined by N_2 adsorption and desorption isotherms using Micrometrics 3Flex. The amount of sample for BET analysis was ~200 mg. Complete degassing of samples at room temperature was checked by monitoring the pressure (< 3 μmHg) over 2 min when the vacuum was temporarily turned off. The result of BET surface area was obtained by analysis of five data points.

High angle annular dark field (HAADF) STEM images and EELS spectra at Ti L-edge were obtained with a JEOL 2100-F transmission electron microscope (200 kV, probe size 0.7-1.0 nm) at the Electron Probe Instrumentation Center (EPIC) at Northwestern University. STEM samples were prepared by sonicating ~3 mg of sample in 10 mL ethanol for 10 min. A drop of the suspension was placed onto a copper grid (Ted Pella, lacey carbon, 300 mesh). The grid was dried in the ambient environment overnight. Average particle size was calculated by counting 200 particles using ImageJ software (Figure S5-S8).

UV-vis spectra were collected with a Shimadzu 3600 UV-visible-NIR spectrophotometer. Cab-O-Sil L90 was used as the reference. All samples were measured in the ambient environment. DRIFTS of adsorbed pyridine was collected on a Nicolet Nexus 670 FTIR spectrometer with a MCT detector and a Harrick reaction cell equipped with KBr windows. Samples were ground into fine powders without dilution. The temperature ramping rate was 5 °C min^{-1}. The background at each temperature, i.e., 180, 120 or 28 °C, was collected under a He flow rate of 25 mL min^{-1} after the temperature was stabilized for 30 min. Pyridine (99.8% anhydrous, Sigma Aldrich) was introduced at 28 °C for 15 min in a He flow of 25 mL min^{-1} through a swath of quartz wool pre-wetted with 0.1 mL of pyridine. The adsorbed pyridine spectra at each temperature were collected 30 min after the temperature was stabilized. Data were taken with 750 scans and a resolution of 4 cm^{-1}, and processed by subtracting the background. The adsorption of 2-propanol followed by pyridine adsorption was only conducted at 180 °C.

Temperature programmed desorption (TPD) of NH_3 or acetone, and temperature programmed reaction (TPRxn) of 2-propanol were conducted with an Altamira AMI-200 instrument equipped with a thermal conductivity detector (TCD) and a mass spectrometer (Universal Gas Analyzer-100). Samples containing Au nanoparticles were pretreated with 50 mL min^{-1} of 10% H_2 in N_2 at 180 °C for 1 h. All samples were dehydrated in 30 mL min^{-1} of He at 200 °C for 2 h before exposed to 60 sequential pulses of 10 % NH_3 in He at 50 °C. There were 2.43 μmol of NH_3 in each pulse. For TPD of NH_3, the sample temperature was ramped to 500 °C at a rate of 30 °C min^{-1} in 40 mL min^{-1} of He and held at 500 °C for 10 min. For 2-propanol TPRxn, a sample was pretreated with 50 mL min^{-1} of 10% H_2 in N_2 at 180 °C for 1 h and cooled down to 40 °C. 2-Propanol was then introduced by bubbling 15 mL min^{-1} of He into a saturator at room temperature for 2 h. The sample temperature was ramped up to 500 °C at a rate of 30 °C min^{-1} in 15 mL min^{-1} of N_2 and held at 500 °C for 6 min. TPD of acetone followed the same procedure as TPRxn of 2-propanol, while TPD of propene was conducted by the same pulsing method as for TPD of NH_3. A calibration curve of known acetone concentrations versus the

corresponding pressures of the mass spectrometer was obtained in He at 15 mL min^{-1}. TPD of acetone was conducted with 15 mL min^{-1} of He using a temperature ramp of 30 °C min^{-1} to 500 °C, and the amount desorbed was calculated using the calibration curve.

X-ray Photoelectron Spectroscopy (XPS) was performed with a Thermo ESCALAB 250Xi equipped with an electron flood gun. The binding energies were calibrated using carbon 1s (284.8 eV). The number of scans and dwell time for N 1s, Au 4f and Ti 2p were 16 and 100 ms. X-ray absorption spectroscopy (XAS) was performed at beamline 5-BMD of the Dupont-Northwestern-Dow Collaborative Access Team (DND-CAT) located in the Advanced Photon Source, Argonne National Laboratory. A Si (1 1 1) monochromator with a resolution of 10^{-4} eV was used. Energies were calibrated with Ti (4966.4 eV) or Au (11918.7 eV) foil. XAS was measured at the Au L_3-edge on fresh catalysts in the transmission mode and on catalysts after reaction in the fluorescence mode under ambient conditions. AuCl and $Au(OH)_3$ as references were measured in the transmission mode. For the Ti K-edge measurements, the catalysts and TS-1 were pretreated in a He flow of 300 mL min^{-1} and a temperature ramping rate of 10 ºC min^{-1} to 180 ºC for 1 h followed by XAS fluorescence collection in He without heating, except TiO_2 anatase was measured in the ambient. XAS data were processed and analyzed by a package software, Demeter [24]. Ti pre-edge peaks were fitted with four Gaussian peaks denoted as A_1, A_2, A_3 and B with an arctan function as a baseline (Figure S9). Theoretical models for Extended X-ray Absorption Fine Structure (EXAFS) fitting were from Atoms.inp Archive [25]. Phase correction was not applied in EXAFS figures and fitting.

3. Results

3.1. Catalyst Structure

BET surface areas of the catalysts are shown in Table 1. Addition of ~1 wt.% Ti caused only small changes in the surface area, suggesting the formation of a well dispersed layer of TiO_x. After addition of ~5 wt.% Ti, the surface area increased by about 20% based on the weight of SiO_2. The adsorption-desorption isotherms showed very small hysteresis loops (Figure 1) as reported by others previously [26], typical for non-porous fume silica consisting of aggregates and agglomerates with mesoscale gaps between 2 to 50 nm. For the higher Ti loading samples 5-Ti/SiO_2 and 4-Ti/[Au/SiO_2], new small pores of 3-7 nm appeared (Figure 2). These data can be explained with a model that TiO_x formed a porous overcoat on the non-porous SiO_2. This was expected due to the relatively low temperatures employed in the catalyst preparation.

STEM images of Au/SiO_2, 1-Ti/[Au/SiO_2], and 4-Ti/[Au/SiO_2] showed small, mostly 1-3 nm diameter, Au particles. Most importantly, addition of TiO_x did not change the average particle size (Table 1). Except for the presence of small Au particles, the morphology of 1-Ti/SiO_2 and 1-Ti/[Au/SiO_2] were similar to that of SiO_2. However, the morphology of 5-Ti/SiO_2 and 4-Ti/[Au/SiO_2] samples showed higher degrees of nonuniformity. There were regions where the surface appeared to be smooth like that of SiO_2, and other regions that were covered with a poorly organized structure (Figure 3). The latter was probably where a thick overlayer of TiO_x was present. Indeed, EELS detected the presence of only a small Ti signal on the smooth region (highlighted with a square in Figure 4) but a strong Ti signal in the poorly organized region (highlighted with a circle).

EELS performed in STEM was used to obtain information on the crystallinity of TiO_x in these samples. It has been shown that the sub-splitting of the Ti L_3 and L_2 transitions, which correspond to transitions from the spin-orbit coupled $2p_{3/2}$ and $2p_{1/2}$ states, respectively and separated by ~5 eV, reflects the degree of crystallinity of the Ti environment because of the crystal-field effect of the coordinating oxygen ions [27]. For Ti atoms in an octahedral environment of oxygen atoms, such as in TiO_2, the Ti 3d states are split into t_{2g} ($3d_\pi$) and e_g ($3d_\sigma$) orbitals. A similar splitting can also be observed at O K-edge due to a transition to O 2p-Ti 3d hybridized states of t_{2g} and e_g symmetry. Both amorphous titanium oxide microtube and Ti_2O_3 showed no sub-splitting of Ti L_2 and L_3 peaks or the peak at O K-edge.[28]

For sample 5-Ti/SiO_2, in the region highlighted with a square, the O K-edge peak due mostly to the amorphous SiO_2 did not show sub-splitting. In the region highlighted with a circle, a strong Ti L-edge peak appeared while the intensity of the O K-edge peak was greatly reduced. Neither the Ti nor the O peaks showed sub-splitting, suggesting that the TiO_x overlayer was amorphous.

Another technique used to gain information on the coordination symmetry of Ti was X-ray absorption, using both the pre-edge features and the EXAFS region of the Ti absorption edge. The pre-edge features of fresh and reaction used catalysts were identical. For TS-1, the pre-edge showed a single, intense absorption peak, while TiO_2 anatase showed four weak features (Figure 5). The spectra of 1-Ti/[Au/SiO_2] and 4-Ti/[Au/SiO_2] showed features that were combinations of TS-1 and anatase, with the anatase feature more prominent in 4-Ti/[Au/SiO_2] than 1-Ti/[Au/SiO_2] (Figure 5), which suggested a higher fraction of O_h Ti in 4-Ti/[Au/SiO_2] than 1-Ti/[Au/SiO_2], and vice versa a higher fraction of T_d Ti in 1-Ti/[Au/SiO_2] than 4-Ti/[Au/SiO_2].

It has been suggested that the Ti pre-edge absorption can be fitted with four Gaussian peaks A_1, A_2, A_3 and B, and the ratio of the area of the A_2 + A_3 peaks, which is a measure of the availability of unoccupied Ti 3d orbitals, to the total area correlates with the area-weighted average peak energy [29, 30]. Furthermore, there is a trend that a lower coordination number showed a higher value of relative area and a lower average pre-edge energy as shown in Figure 6. After fitting the data in Figure 5 with these four peaks (Figure S9), the results were used to calculate the points for 1-Ti/[Au/SiO_2], 4-Ti/[Au/SiO_2], and TiO_2(anatase) in Figure 6. Using this correlation, the Ti in both 1-Ti/[Au/SiO_2] and 4-Ti/[Au/SiO_2] had an average coordination close to 5. This suggested a mixture of T_d and O_h Ti, consistent with conclusions from the preedge features and the presence of an amorphous TiO_x overlayer.

Fitting of the first shell coordination data in EXAFS for both 1-Ti/[Au/SiO_2] and 4-Ti/[Au/SiO_2] also showed a coordination number of ~5 (Table 2 and Figure S10). However, the Ti-O bond distance of 4-Ti/[Au/SiO_2] (1.91 Å) was longer than 1-Ti/[Au/SiO_2] (1.85 Å). No obvious Ti-O-Ti shells scattering was observed for these two samples.

After reaction, the Au nanoparticles remained metallic on the catalysts (Figure S11) and EXAFS fitting results of the Au edge showed similar average distances (2.84-2.85 Å) between Au atoms on all the Au catalysts (Table 2 and Figures S12). Within experimental uncertainties, the nearest neighbor coordination number was the same on all samples with values consistent with the STEM results, and in agreement with literature results that Au-Au nearest neighbor distance of 2.84-2.85 Å would have N_{Au-Au} in the range of 8.5-10 and correspond to particle size of 1.5-3.2 nm [31].

Finally, DR-UV-vis spectroscopy was also used to investigate the structural properties of the catalysts, making use of the absorption in the near UV region that offers information on the coordination environments of TiO_x species. For TS-1 (Figure 7), an intense peak appeared at ~220 nm due to the ligand-to-metal charge transfer (LMCT) transition of isolated tetrahedral TiO_4 units [32, 33]. Bulk TiO_2 anatase, where Ti is in an octahedral coordination, showed an absorption peak at ~320 nm. The absorption peaks of 1-Ti/SiO_2 and 1-Ti/[Au/SiO_2] were at 260-280 nm, while those of 5-Ti/SiO_2 and 4-Ti/[Au/SiO_2] were at 280-300 nm. They were in the range for samples containing pentacoordinated Ti species, oligomeric species, and TiO_2 nanoclusters [32, 33]. The longer wavelengths for 5-Ti/SiO_2 and 4-Ti/[Au/SiO_2] suggested that these samples contained higher fractions of oligomeric Ti species than 1-Ti/SiO_2 and 1-Ti/[Au/SiO_2].

The Au-containing samples also showed a broad peak at 520-550 nm due to the size- and support-dependent surface plasmon vibration of Au nanoparticles [34]. For Au/SiO_2 and 1-Ti/[Au/SiO_2], the peaks centered at ~520 nm. For 4-Ti/[Au/SiO_2], the peak was at 550 nm and broader. Assuming that the STEM and EXAFS data were accurate, that the average Au particle size were the same for all Au sample, the shift in the plasmon peak for 4-Ti/[Au/SiO_2] would be a results of the more prominent TiO_x overlayer on Au.

3.2. Ti Oxidation States and Catalyst Acidity

To determine if there was a mixture of oxidation states of Ti species in the amorphous TiO_x, XPS spectra were collected on the supported Au catalysts. From the literature, the Ti 2p XPS spectrum for TiO_2 shows two peaks due to spin-orbit splitting into $2p_{3/2}$ and $2p_{1/2}$ states at 458.8 eV and 464.5 eV, respectively [35]. The binding energies of the Ti $2p_{3/2}$ peaks of TiO (Ti^{2+}) and Ti_2O_3 (Ti^{3+}) are at ~456 eV and ~457 eV, respectively [28, 35]. For samples 1-Ti/[Au/SiO_2] and 4-Ti/[Au/SiO_2], the Ti $2p_{3/2}$ and $2p_{1/2}$ peaks were at 459-459.5 and 465 eV, respectively (Figure 8). The slightly higher binding energy for the $2p_{3/2}$ peak than in the literature could be instrument error, or it could be due to contribution from a small quantity of tetrahedral Ti species

on silica that has been assigned to a Ti $2p_{3/2}$ peak at ~460 eV [36]. Overall, the results indicated that there was little TiO (Ti^{2+}) or Ti_2O_3 (Ti^{3+}) in these supported Au catalysts, and the Ti in these samples were Ti^{4+}.

Two methods were used to probe acidity of these catalysts: adsorption of pyridine monitored with DRIFTS [37] and adsorption and TPD of NH_3. No Brønsted acid sites, detected as pyridinium ions (BPy) at ~1540 (ν19b) and ~1640 cm^{-1} (ν8a) were observed on any of the samples. Pyridine bound to Lewis acid sites (LPy) at ~1445 (ν19b) and ~1608 cm^{-1} (ν8a) were observed on catalysts containing TiO_x species (Figures 9, S13, and S14). We also observed a 1488 cm^{-1} band commonly assigned to the vibrations of both BPy and LPy [38-40], and bands due to physisorbed (PPy), hydrogen-bonded (HPy) and gas phase pyridine (GPy). Table 3 summarizes the DRIFTS results. Whereas intensities of the peaks were much stronger for the higher Ti loading samples, the presence of Au did not have much effect. In general, the GPy, PPy, and HPy peaks gradually decreased or disappeared as the samples were purged with He at 28 °C or by heating to 120 ºC and higher (Figures 9, S13, S14). The decrease in the HPy peak at 1596 cm^{-1} made the LPy peak at 1608 cm^{-1} (ν8a) much more apparent. After heating to 180 °C, only LPy peaks remained. On Au/SiO_2, no LPy peaks were detected after heating to 120 °C or 180 °C.

To determine whether adsorbed 2-propanol or water could convert a Lewis acid site into a Brønsted acid site [41], pyridine was introduced after adsorption of 2-propanol at 180 °C. The sample cell was then purged with He, and DRFIT spectrum was collected after 15 min. Only peaks attributed to LPy at 1447 and 1606 cm^{-1} were observed and no BPy peaks (Figure 10). Thus, there should be no Brønsted acid sites present under our reaction conditions.

The amounts of NH_3 adsorbed from a pulse passed over the catalysts at 50 °C are shown in Table 6. SiO_2 adsorbed 110 μmol g^{-1} of NH_3 (~1.2 μmol m^{-2}), probably resulting from hydrogen bonding with SiOH groups because TPD-NH_3 barely showed a desorption peak. By subtracting this value from the total amount of NH_3 adsorbed, then the addition of Au nanoparticles resulted in an additional adsorption of 119 μmol g^{-1} on Au/SiO_2. For the other samples, the additional amounts adsorbed were 217, 703, 288, and 1002 μmol g^{-1} for 1-Ti/SiO_2, 5-Ti/SiO_2, 1-$Ti/[Au/SiO_2]$, and 4-$Ti/[Au/SiO_2]$, respectively. By further expressing these values on the basis of per gram of SiO_2, and subtracting contributions from both Au and SiO_2, then the addition of Ti resulted in roughly 200±20 μmol g^{-1} SiO_2 for adding ~1 wt.% Ti, and roughly 810±100 μmol g^{-1} for adding 4-5 wt.% Ti.

TPD of these adsorbed NH_3 showed very broad peaks for all catalysts, and the peak maximum varied slightly (Figure 11). For 1-Ti/SiO_2, 5-Ti/SiO_2, 1-$Ti[Au/SiO_2]$, and 4-$Ti/[Au/SiO_2]$, the maximum appeared at 190 °C, 220 °C, 175 °C and 240 °C, respectively. That is, the peak maximum was at a higher temperature for the higher Ti loading samples, which

might be due to readsorption of desorbed NH_3, which would be more severe for higher Ti loading samples. Thus, overall, the samples showed similar distributions of Lewis acid strengths.

3.3. TPRxn of 2-Propanol and TPD of Acetone and Propene

Under the conditions of TPD experiments, there was no evidence of propene adsorption on these catalysts, suggesting that propene interacted weakly. TPD of acetone showed a peak at 140°C on all the three catalysts containing Au (Figure 12). The activation energy for desorption of acetone could be calculated from the peak temperature assuming uniform sites and a desorption kinetic that is first-order in the surface density of acetone [42, 43]. Table 4 summarizes the calculated activation energies for acetone desorption for different values of *ν*, the pre-exponential factor for desorption. The ratios of moles of acetone desorbed to surface Au were 4-6 for all the three catalysts containing Au (Table 5).

$$\frac{E_{a,des}}{RT_p^2} = \frac{\nu}{\beta}\exp\left(\frac{-E_{a,des}}{RT_p}\right),$$

where $E_{a,des}$ is the activation energy for desorption, R is ideal gas constant, T_p is the desorption peak temperature, *ν* is the pre-exponential factor for desorption and β is the heating rate.

TPRxn of adsorbed 2-PrOH produced different products from different catalysts. On SiO_2, only propene evolution was observed as a broad, low intensity peak with a maximum at around 130 °C (not shown). Propene was also the only product detected on 1-Ti/SiO_2 and 5-Ti/SiO_2, and the peak maxima were at 270 °C and 230 °C respectively (Figure 13). Small amounts of propene were observed on Au/SiO_2, 1-Ti and 4-Ti/[Au/SiO_2] at ~140 ºC. For the latter two samples, there were additional propene peaks at temperatures similar to those from 1-Ti/SiO_2 and 5-Ti/SiO_2. The higher temperature peak was about the same area as the lower temperature peak on 1-Ti/[Au/SiO_2], but was significantly larger for 4-Ti/[Au/SiO_2].

In addition to propene, acetone was also evolved on the Au-containing samples (Figure 14). On Au/SiO_2, acetone was evolved at 130-140°C, which was the same as the TPD peak of acetone. Two acetone peaks were observed for both 1-Ti/[Au/SiO_2] and 4-Ti/[Au/SiO_2]. There was a much smaller peak at 130-140ºC, and a much larger peak at 240-260°C.

3.4. Catalytic Decomposition of 2-Propanol

Catalytic 2-propanol decomposition was conducted between 170-190 ºC, where reasonable conversions and product analyses could be obtained. Table 6 shows the results at 190 ºC for all the catalysts, collected using different catalyst weights in order to maintain <16% conversions. Results for other reaction conditions are shown in Supplementary Figure S15.

Without Au, only propene was detected on 1-Ti/SiO_2 and 5-Ti/SiO_2 as expected [44-46], and its rate of formation, when compared using a common basis of unit weight of SiO_2, increased roughly proportionally with Ti loading. Acetone became the predominant product on all Au-containing catalysts. On Au/SiO_2, acetone selectivity reached 92%. Addition of TiO_x to Au/SiO_2 increased its activity for both acetone and propene formation. The propene formation rate was roughly proportional to the TiO_x loading, but the acetone formation rate increased less rapidly. Consequently, the selectivity for acetone decreased with increasing Ti loading. Since Au/SiO_2 without Ti had only a small activity for acetone formation, the data indicated that sites composed of both Au and TiO_x, such as the Au-TiO_x interfacial perimeter sites, were responsible for the majority of acetone formation.

The dependence of 2-propanol decomposition rate on the partial pressures of 2-propanol are shown in Figures 15. On 1-Ti/SiO_2 and 5-Ti/SiO_2, where only propene was formed, the rate of 2-propanol decomposition was rather independent of 2-propanol partial pressure. On the other hand, both Ti/[Au/SiO_2] catalysts showed a positive order dependence for propene formation on propanol partial pressure. The order was positive (0.2-0.4) at lower pressures, and decreased to near zeroth order at higher pressures (Figure 16). The order for propene formation rates on Au/SiO_2 was slightly higher (0.5-0.7).

Because acetone was the major product on the Au-containing catalysts, the dependence of the overall 2-propanol decomposition rate and acetone formation rate on partial pressures of 2-propanol (Figure 15 and 16) were rather similar. Au/SiO_2 showed an order of 0.4 in both rates. On both Ti/[Au/SiO_2] catalysts, the order dependence was 0.7-1.1 at low 2-propanol pressures and reached zero and even slightly negative at higher pressures.

Because the reaction rates depended on 2-propanol pressure, the apparent activation energy E_a also depended on the propanol pressure. For comparison among catalysts, the condition of zeroth order dependence of 2-propanol pressure (P= 5.6 kPa) was chosen to determine E_a by varying the temperature and measuring the reaction rates. Although Au/SiO_2 did not achieve zero order reaction, the reaction rates at this same pressure was used. The obtained E_a's and preexponential factors for the overall reaction, acetone and propene formation are shown in Table 7.

Because the main reaction for the Au-containing catalysts was acetone formation, values for ln (A) and E_a for the overall reaction and acetone formation were similar for each of the catalysts. However, although the E_a for acetone formation for 1-Ti/[Au/SiO_2] and 4-Ti/[Au/SiO_2] were similar, they were substantially higher than that for Au/SiO_2. Since the E_a for propene formation were smaller than for acetone formation, these larger E_a's could not be due to contribution from propene formation. Instead, they must indicate different active sites. Similarly, the E_a for propene formation on the two Au-containing catalysts were substantially smaller than those on Ti/SiO_2. This implied that the properties of the active sites or the reactive intermediate involved were different.

3.5. Catalytic 2-propanol Oxidation with O_2

Addition of O_2 in the feed increased the activities of the Au-containing catalysts but not for the Ti/SiO_2 catalysts. For the Au-containing catalysts, the 2-propanol conversion increased with time-on-stream for the first 2-3 h before reaching a steady state. For example, at 30 min, the conversions for Au/SiO_2 and 1-$Ti/[Au/SiO_2]$ were 11% and 14%, respectively. At steady state, Au/SiO_2 reached a conversion of ~40%, and 1-$Ti/[Au/SiO_2]$ reached ~20%.

The product selectivities were little affected by the addition of O_2. On 1-Ti/SiO_2 and 5-Ti/SiO_2, propene was the only product. For the Au-containing catalysts, acetone was the major product accompanied with significant amounts of water production, indicating oxidative dehydrogenation. In fact, on both 1-$Ti/[Au/SiO_2]$ and 4-$Ti/[Au/SiO_2]$ the selectivities for acetone increased with O_2 present (Table 8).

4. Discussion

Results of various characterization suggested that the catalysts contained 1-3 nm Au nanoparticles on a nonporous SiO_2 support. The samples were covered by an overlayer of amorphous TiO_2, which XPS showed to consist of all Ti(IV). At high Ti loadings, the Ti coverage was nonuniform, there were regions of thick TiO_2 patches independent of whether Au particles were present or not, and microdomains of crystalline TiO_2 began to appear. The Ti ions in the overlayer were present in roughly equal amounts of T_d and O_h coordination, such that the average coordination number was about 5. This model was derived from corroborative results from EELS, EXAFS, XANES, and DR-UV-vis measurements. Horváth et al.[47] prepared a TiO_2-decorated Au/SiO_2 using a different Ti precursor than ours and colloidal Au particles but otherwise a similar method of impregnation of Ti onto Au/SiO_2. They also observed TiO_2 dispersed over all surfaces of the catalyst.

Only Lewis acid and no Brønsted acid sites were detected on all samples using pyridine as the probe molecule. The presence of 2-PrOH did not change the type of sites available, and no new sites were formed. These Lewis acid sites were associated with the TiO_2 overlayer and were the main source of propene formation from 2-PrOH, since they were present in catalysts without Au, and could account for the formation of propene on all the catalysts. However, it is interesting to note that the apparent activation energy for propene formation was higher on the two Ti/SiO_2 catalysts than on the two $Ti/[Au/SiO_2]$ catalysts. We attribute this to the fact that on the Au-containing catalysts, there are two competing pathways for an adsorbed 2-propoxy, namely to form acetone versus propene. This will be discussed further later.

Acetone was formed only on Au-containing catalysts. Thus, Au must be responsible for cleavage of the α-C-H bond of the adsorbed 2-propoxy. Since the rates of acetone formation on the two $Ti/[Au/SiO_2]$ catalysts were much higher than that on Au/SiO_2, and the catalyst with a higher Ti loading was the most active, it can be concluded that acetone formation was facilitated by the simultaneous presence of TiO_2 and Au, such as at the interfacial perimeter sites. Thus, for these two catalysts, 2-propoxide was formed by dissociative adsorption of 2-propanol on the TiO_2 at the interfacial perimeter site. This was followed by cleavage of the α-C-H bond by the Au atom to form adsorbed acetone, which desorbed as the product (Figure 17B). Recent studies

also reported the formation of acetone after the introduction of Au nanoparticles onto TiO_2 and γ-Al_2O_3 [17, 19].

Adsorbed acetone desorbed at the same temperature of ~140 °C in TPD on all Au-containing catalysts (Figure 12), which was lower than the reaction temperatures of 170-190 °C. Assuming a first order desorption kinetics for adsorbed acetone and a pre-exponential factor of 10^{11} - 10^{12} min^{-1}, the desorption activation energy was 85 - 93 kJ mol^{-1} (Table 4). This is lower than the apparent acetone formation activation energy of 94-105 kJ mol^{-1} for 1-Ti/[Au/SiO_2] and 4-Ti/[Au/SiO_2] (Table 7). These suggest α-C-H bond cleavage is the rate-limiting step in 2-PrOH decomposition. The addition of O_2 to the feed increased the acetone formation rate substantially. Since desorption of acetone is not expected to be affected by O_2, but α-C-H bond cleavage could be affected by the presence of adsorbed O on Au, either by enabling the formation of Au-OH or changing the electron density at the Au atom, the observation of substantial rate enhancement by O_2 supports α-C-H bond cleavage to be the rate limiting step.

In the absence of Ti, on the other hand, the activation energy for acetone formation over Au/SiO_2 was only 66 kJ mol^{-1}, higher than its desorption activation energy (55 kJ mol^{-1}) with a similar pre-exponential factor. The very different apparent E_a than those for Ti/[Au/SiO_2] suggested that the active sites were different on these catalysts, further supporting the model that on Ti/[Au/SiO_2] catalysts, acetone formation was at the interfacial perimeter sites. It also suggested a different reaction pathway on Au/SiO_2. One possible mechanism is shown in Figure 17A. 2-Propanol is adsorbed on Au followed by α-C-H bond cleavage, and cleavage of O-H bond is the rate limiting step. Isotope labeling experiments could be used to test this proposal.

Whereas TPRxn of 2-PrOH on Au/SiO_2 showed only one acetone formation peak, a second, higher temperature peak was observed for 1-Ti/[Au/SiO_2] and 4-Ti/[Au/SiO_2]. We believe that the higher temperature peak is from the Au-TiO_x interfacial perimeter sites, as its intensity increased with Ti content.

Propene formation took place readily on Lewis acid sites on the TiO_2 overlayer, and the rate increased with increasing Ti content. The activity on the TiO_2 overlayer was sufficient to account for the propene formation on both 1-Ti/[Au/SiO_2] and 4-Ti/[Au/SiO_2]. Thus, there is no evidence that propene was formed on the Au surface or the interfacial perimeter sites. It is interesting that the 2-propanol partial pressure dependence of propene formation was different on samples with and without Au. Without Au, the dependence was nearly zero order, and with Au, there was a small positive order. It is possible that the apparent positive order on Au-containing catalysts was due to the order dependence of faster acetone formation, which competes for adsorbed 2-propoxide. This would be possible if the adsorbed 2-propoxide is mobile on the surface and diffuses among different sites. It is also interesting to note that under our conditions, TiO_2 was nearly inactive even taking into account the surface area. This suggests that O_h Ti is much less active than Ti of a lower coordination.

The results of this study provide further support of the previous conclusion that the interfacial perimeter sites are essential for selective acetone formation in the oxidation of propane in the presence of a H_2/O_2 mixture.[9, 10] They offer additional insight on the possible reaction mechanism for that reaction. It is likely that adsorbed O or hydroperoxide (-OOH) on

Au is essential in the first step of propane activation by cleaving the O-H bond to form Au-OH and adsorbed propoxide on TiO_x at the interface. The propoxide then reacts in the same manner as in this reaction.

5. Conclusions

We have demonstrated the formation of acetone on Au-containing catalysts from adsorbed 2-propoxide, the rate of which is facilitated by the presence of a porous, amorphous TiO_2 overlayer on Au. The high activity in the simultaneous presence of Au and amorphous TiO_2 substantiates the importance of Au-TiO_2 interfacial perimeter sites for this reaction. The data imply that Au at the interfacial perimeter site is responsible for α-C-H bond scission, which is the rate limiting step. This step is facilitated by the presence of O_2, suggesting that it is assisted by adsorbed O_2 on Au via enabling the formation of Au-OH. The fact that Au/SiO_2 is capable of forming acetone also suggests that TiO_2 is not critical, and other oxides may also be effective. Perhaps TiO_2 is an attractive support because it easily forms an overlayer on Au, which results in a high density of interfacial perimeter sites and thus a highly active catalyst. The results gathered and the understanding derived could help future development of Au catalyst for hydrocarbon conversions.

Acknowledgement

The authors acknowledge financial support from Institute for Catalysis in Energy Processes supported by the U.S. Department of Energy, Office of Science, Office of Basic Energy Sciences under Award Number DOE DE-FG02-03-ER15457. The following facilities at Northwestern University were used in this work: the EPIC, Keck-II, and/or SPID facility(ies) of the NUANCE Center, which received support from the Soft and Hybrid Nanotechnology Experimental (SHyNE) Resource (NSF ECCS-1542205), the MRSEC program (NSF DMR-1121262) at the Materials Research Center, the International Institute for Nanotechnology (IIN), the Keck Foundation, and the State of Illinois, through the IIN; the J.B. Cohen X-Ray Diffraction Facility supported by the MRSEC program of the National Science Foundation (DMR- 1121262); DND-CAT located at Sector 5 of the Advanced Photon Source (APS), whichis supported by Northwestern University, E.I. DuPont de Nemours & Co., and The Dow Chemical Company; the Advanced Photon Source, a U.S. Department of Energy (DOE) Office of Science user facility operated for the DOE Office of Science by the Argonne National Laboratory under Contract No. DE-AC02-06CH11357; the CleanCat Core facility funded by the U.S. Department of Energy (DE-FG02-03ER15457); and the Quantitative Bio-element Imaging Center. The authors also would like to thank Dr. Neil M. Schweitzer for discussion and experimental assistance, Professor Justin Notestein for use of the DR-UV-vis spectrometer, and Dr. Qing Ma at the DuPont-Northwestern-Dow Collaborative Access Team (DND-CAT) for discussion and experimental assistance.

6. References

[1] X. Yang, X. Wang, C. Liang, W. Su, C. Wang, Z. Feng, C. Li, J. Qiu, Aerobic oxidation of alcohols over Au/TiO2: An insight on the promotion effect of water on the catalytic activity of Au/TiO2, Catal. Commun., 9 (2008) 2278-2281.
[2] M. Turner, V.B. Golovko, O.P.H. Vaughan, P. Abdulkin, A. Berenguer-Murcia, M.S. Tikhov, B.F.G. Johnson, R.M. Lambert, Selective oxidation with dioxygen by gold nanoparticle catalysts derived from 55-atom clusters, Nature, 454 (2008) 981-983.
[3] B. Taylor, J. Lauterbach, G.E. Blau, W.N. Delgass, Reaction kinetic analysis of the gas-phase epoxidation of propylene over Au/TS-1, J. Catal., 242 (2006) 142-152.
[4] M. Haruta, B. Uphade, S. Tsubota, A. Miyamoto, Selective oxidation of propylene over gold deposited on titanium-based oxides, Res. Chem. Intermed., 24 (1998) 329-336.
[5] J. Jiang, H. Kung, M. Kung, J. Ma, Aqueous phase epoxidation of 1-butene catalyzed by suspension of Au/TiO2 +TS-1, Gold Bull., 42 (2009) 280-287.
[6] K.K.B. J. J. Bravo-Suarez, T. Akita, T. Fujitani, T. J. Fuhrer and S. T. Oyama, <Propane reacts with O2 and H2 on gold supported TS-1 to form oxygenates with high selectivity.pdf>, Chem. Commun., (2008) 3272-3274.
[7] J.J. Bravo-Suarez, K.K. Bando, T. Fujitani, S.T. Oyama, Mechanistic study of propane selective oxidation with H-2 and O-2 on Au/TS-1, J. Catal., 257 (2008) 32-42.
[8] J.J. Bravo-Suárez, K.K. Bando, J. Lu, T. Fujitani, S.T. Oyama, Oxidation of propane to propylene oxide on gold catalysts, J. Catal., 255 (2008) 114-126.
[9] Y.Y. Wu, N.A. Mashayekhi, H.H. Kung, Au-metal oxide support interface as catalytic active sites, Catal. Sci. Technol., 3 (2013) 2881-2891.
[10] N.A. Mashayekhi, Y.Y. Wu, M.C. Kung, H.H. Kung, Metal nanoparticle catalysts decorated with metal oxide clusters, Chem. Commun., 48 (2012) 10096-10098.
[11] D. Courcot, B. Grzybowska, Y. Barbaux, M. Rigole, A. Ponchel, M. Guelton, Effect of potassium addition to the TiO2 support on the structure of V2O5/TiO2 and its catalytic properties in the oxidative dehydrogenation of propane, Journal of the Chemical Society, Faraday Transactions, 92 (1996) 1609-1617.
[12] F.M. Bautista, J.M. Campelo, D. Luna, J. Luque, J.M. Marinas, Gas-phase selective oxidation of toluene on TiO2-sepiolite supported vanadium oxides, Catalysis Today, 128 (2007) 183-190.
[13] K.S. Kim, M.A. Barteau, Reactions of aliphatic alcohols on the {011}-facetted titanium dioxide (001) surface, J. Mol. Catal., 63 (1990) 103-117.
[14] K.S. Kim, M.A. Barteau, W.E. Farneth, Adsorption and decomposition of aliphatic alcohols on titania, Langmuir, 4 (1988) 533-543.
[15] O. Bondarchuk, Y.K. Kim, J.M. White, J. Kim, B.D. Kay, Z. Dohnalek, Surface Chemistry of 2-Propanol on TiO2(110): Low- and High-Temperature Dehydration, Isotope Effects, and Influence of Local Surface Structure, J. Phys. Chem. C, 111 (2007) 11059-11067.
[16] E. Farfan-Arribas, R.J. Madix, Role of defects in the adsorption of aliphatic alcohols on the TiO2(110) surface, Journal of Physical Chemistry B, 106 (2002) 10680-10692.
[17] M.C. Holz, K. Kahler, K. Tolle, A.C. van Veen, M. Muhler, Gas-phase oxidation of 2-propanol over Au/TiO2 catalysts to probe metal-support interactions, Phys. Status Solidi B, 250 (2013) 1094-1106.

[18] D.V. Potapenko, Z. Li, Y. Lou, Y. Guo, R.M. Osgood Jr, 2-Propanol reactivity on in situ prepared Au(1 1 1)-supported TiO2 nanocrystals, J. Catal., 297 (2013) 281-288.
[19] Z. Martinez-Ramirez, J.A. Gonzalez-Calderon, A. Almendarez-Camarillo, J.C. Fierro-Gonzalez, Adsorption and dehydrogenation of 2-propanol on the surface of γ-Al2O3-supported gold, Surf. Sci., 606 (2012) 1167-1172.
[20] B.P. Block, J.C. Bailar, The Reaction of Gold(III) with Some Bidentate Coördinating Groups1, J. Am. Chem. Soc., 73 (1951) 4722-4725.
[21] R. Zanella, A. Sandoval, P. Santiago, V.A. Basiuk, J.M. Saniger, New preparation method of gold nanoparticles on SiO2, J. Phys. Chem. B, 110 (2006) 8559-8565.
[22] L.T. Zhuravlev, Concentration of hydroxyl groups on the surface of amorphous silicas, Langmuir, 3 (1987) 316-318.
[23] G.S. Parks, B. Barton, VAPOR PRESSURE DATA FOR ISOPROPYL ALCOHOL AND TERTIARY BUTYL ALCOHOL, J. Am. Chem. Soc., 50 (1928) 24-26.
[24] B. Ravel, M. Newville, ATHENA, ARTEMIS, HEPHAESTUS: data analysis for X-ray absorption spectroscopy using IFEFFIT, Journal of Synchrotron Radiation, 12 (2005) 537-541.
[25] M. Newville, Atoms.inp Archive: Crystallographic Data from GSECARS.
[26] V.M. Gun'ko, I.F. Mironyuk, V.I. Zarko, E.F. Voronin, V.V. Turov, E.M. Pakhlov, E.V. Goncharuk, Y.M. Nychiporuk, N.N. Vlasova, P.P. Gorbik, O.A. Mishchuk, A.A. Chuiko, T.V. Kulik, B.B. Palyanytsya, S.V. Pakhovchishin, J. Skubiszewska-Zięba, W. Janusz, A.V. Turov, R. Leboda, Morphology and surface properties of fumed silicas, J. Colloid Interface Sci., 289 (2005) 427-445.
[27] G. Bertoni, E. Beyers, J. Verbeeck, M. Mertens, P. Cool, E.F. Vansant, G. Van Tendeloo, Quantification of crystalline and amorphous content in porous TiO2 samples from electron energy loss spectroscopy, Ultramicroscopy, 106 (2006) 630-635.
[28] C.-N. Huang, J.-S. Bow, Y. Zheng, S.-Y. Chen, N. Ho, P. Shen, Nonstoichiometric Titanium Oxides via Pulsed Laser Ablation in Water, Nanoscale Research Letters, 5 (2010) 972-985.
[29] T.R. Eaton, M.P. Campos, K.A. Gray, J.M. Notestein, Quantifying accessible sites and reactivity on titania–silica (photo)catalysts: Refining TOF calculations, J. Catal., 309 (2014) 156-165.
[30] J.M. Notestein, L.R. Andrini, V.I. Kalchenko, F.G. Requejo, A. Katz, E. Iglesia, Structural Assessment and Catalytic Consequences of the Oxygen Coordination Environment in Grafted Ti−Calixarenes, J. Am. Chem. Soc., 129 (2007) 1122-1131.
[31] J.T. Miller, A.J. Kropf, Y. Zha, J.R. Regalbuto, L. Delannoy, C. Louis, E. Bus, J.A. van Bokhoven, The effect of gold particle size on AuAu bond length and reactivity toward oxygen in supported catalysts, J. Catal., 240 (2006) 222-234.
[32] F. Berube, B. Nohair, F. Kleitz, S. Kaliaguine, Controlled Postgrafting of Titanium Chelates for Improved Synthesis of Ti-SBA-15 Epoxidation Catalysts, Chem. Mater., 22 (2010) 1988-2000.
[33] L. Raboin, J. Yano, T.D. Tilley, Epoxidation catalysts derived from introduction of titanium centers onto the surface of mesoporous aluminophosphate: Comparisons with analogous catalysts based on mesoporous silica, J. Catal., 285 (2012) 168-176.
[34] E. Sacaliuc, A.M. Beale, B.M. Weckhuysen, T.A. Nijhuis, Propene epoxidation over Au/Ti-SBA-15 catalysts, J. Catal., 248 (2007) 235-248.
[35] N. Kruse, S. Chenakin, XPS characterization of Au/TiO2 catalysts: Binding energy assessment and irradiation effects, Applied Catalysis A: General, 391 (2011) 367-376.

[36] S. Sakugawa, K. Wada, M. Inoue, Ti-bridged silsesquioxanes as precursors of silica-supported titanium oxide catalysts for the epoxidation of cyclooctene, J. Catal., 275 (2010) 280-287.
[37] M.I. Zaki, M.A. Hasan, F.A. Al-Sagheer, L. Pasupulety, In situ FTIR spectra of pyridine adsorbed on SiO2–Al2O3, TiO2, ZrO2 and CeO2: general considerations for the identification of acid sites on surfaces of finely divided metal oxides, Colloids and Surfaces A: Physicochemical and Engineering Aspects, 190 (2001) 261-274.
[38] M. Tamura, K.-i. Shimizu, A. Satsuma, Comprehensive IR study on acid/base properties of metal oxides, Appl. Catal., A, 433 (2012) 135-145.
[39] S.M. Jung, P. Grange, TiO2–SiO2 mixed oxide modified with H2SO4: II. Acid properties and their SCR reactivity, Applied Catalysis A: General, 228 (2002) 65-73.
[40] B. Notari, R.J. Willey, M. Panizza, G. Busca, Which sites are the active sites in TiO2–SiO2 mixed oxides?, Catal. Today, 116 (2006) 99-110.
[41] A.P. Kulkarni, D.S. Muggli, The effect of water on the acidity of TiO2 and sulfated titania, Applied Catalysis A: General, 302 (2006) 274-282.
[42] X. Xia, J. Strunk, S. Litvinov, M. Muhler, Influence of Re-adsorption and Surface Heterogeneity on the Microkinetic Analysis of Temperature-Programmed Desorption Experiments, J. Phys. Chem. C, 111 (2007) 6000-6008.
[43] P.A. Redhead, Thermal desorption of gases, Vacuum, 12 (1962) 203-211.
[44] Z.F. Liu, J. Tabora, R.J. Davis, RELATIONSHIPS BETWEEN MICROSTRUCTURE AND SURFACE-ACIDITY OF TI-SI MIXED-OXIDE CATALYSTS, Journal of Catalysis, 149 (1994) 117-126.
[45] A. Gervasini, J. Fenyvesi, A. Auroux, Study of the acidic character of modified metal oxide surfaces using the test of isopropanol decomposition, Catal. Lett., 43 (1997) 219-228.
[46] D. Haffad, A. Chambellan, J.C. Lavalley, Propan-2-ol transformation on simple metal oxides TiO2, ZrO2 and CeO2, J. Mol. Catal. A, 168 (2001) 153-164.
[47] A. Horváth, A. Beck, A. Sárkány, G. Stefler, Z. Varga, O. Geszti, L. Tóth, L. Guczi, Silica-Supported Au Nanoparticles Decorated by TiO2: Formation, Morphology, and CO Oxidation Activity, J. Phys. Chem. B, 110 (2006) 15417-15425.

Figure captions:

Figure 1. N_2 adsorption isotherms of catalysts. The isotherms are vertically displaced for clarity.

Figure 2. Barrett-Joyner-Halenda (BJH) pore size distributions. The bottom panel emphasizes the smaller diameter region.

Figure 3. STEM images of (a) Au/SiO_2, (b) 1-Ti/[Au/SiO_2], (c) 4-Ti/[Au/SiO_2] and (d) 5-Ti/SiO_2 The STEM images were collected on catalysts after 2-propanol decomposition.

Figure 4. 5-Ti/SiO_2 after ozone treatment at 150 °C. (a) STEM image and (b) EELS spectra with the corresponding areas in the circle and square.

Figure 5. Pre-edge features of the Ti K-edge of the catalysts.

Figure 6. The relative area of peaks $(A_2 + A_3)/A_T$ versus area-weighted average pre-edge energy, determined by the positions of A_2 and A_3. TS-1 (empty triangle), 1-Ti/[Au/SiO_2], 4-Ti/[Au/SiO_2] (solid circle) and anatase (solid triangle) in this study are plotted. Ba_2TiO_4 (empty circle), fresnoite (empty square) and anatase (cross) are taken from Todd et al.[29] A_T is the total area of pre-edge peaks ($A_T=A_1 + A_2 + A_3 + A_B$).

Figure 7. DR-UV-vis spectra of catalysts after reaction.

Figure 8. XPS of Ti 2p spectra for 1-Ti/[Au/SiO_2] and 4-Ti/[Au/SiO_2]. The samples had been treated with 300 cm^3 min^{-1} of 10% O_3/O_2 at 150 °C as part of the preparation procedure, and 50 cm^3 min^{-1} of 10% H_2/He at 180 °C for 1 h pretreatment before catalytic tests. They were exposed to air for XPS measurement.

Figure 9. DRIFT spectra with pyridine adsorption on 1-Ti/[Au/SiO_2] and 4-Ti/[Au/SiO_2].

Figure 10. DRIFT spectra of 4-Ti/[Au/SiO_2] after adsorption of 2PrOH at 180 °C followed by exposure to pyridine at the same temperature. The spectrum was collected after He purging at 25 mL/min for 15 min.

Figure 11. TPD-NH_3 spectra monitored with a mass spectrometer on (a) 1-Ti/SiO_2 and 5-Ti/SiO_2 (b) SiO_2, Au/SiO_2, 1-Ti[Au/SiO_2] and 4-Ti/[Au/SiO_2].

Figure 12. TPD of acetone on Au/SiO_2, 1-Ti/[Au/SiO_2] and 4-Ti/[Au/SiO_2].

Figure 13. Propene evolution during TPRxn of 2-PrOH.

Figure 14. Acetone evolution during TPRxn of 2-propanol.

Figure 15. Dependence of 2-propanol decomposition rates on the partial pressure of 2-propanol on (a) 1-Ti/SiO_2, (b) 5-Ti/SiO_2, (c) Au/SiO_2, (d) 1-Ti/[Au/SiO_2], and (e) 4-Ti/[Au/SiO_2]. For

both d and e, the rates shown are the observed rate minus the rates on Au/SiO_2. n is the reaction order obtained from the slopes.

Figure 16. Dependence of propene (a, c, and e) and acetone (b, d, and f) production rates on the partial pressure of 2-propanol on (a, b) Au/SiO_2, (c, d) 1-Ti/[Au/SiO_2], and (e, f) 4-Ti/[Au/SiO_2]. For c, d, e, and f, the rates shown are the observed rate minus the rates on Au/SiO_2. n is the reaction order obtained from the slopes.

Figure 17. 2-propanol decomposition on (A) Au/SiO_2 and (B) Ti/[Au/SiO_2].

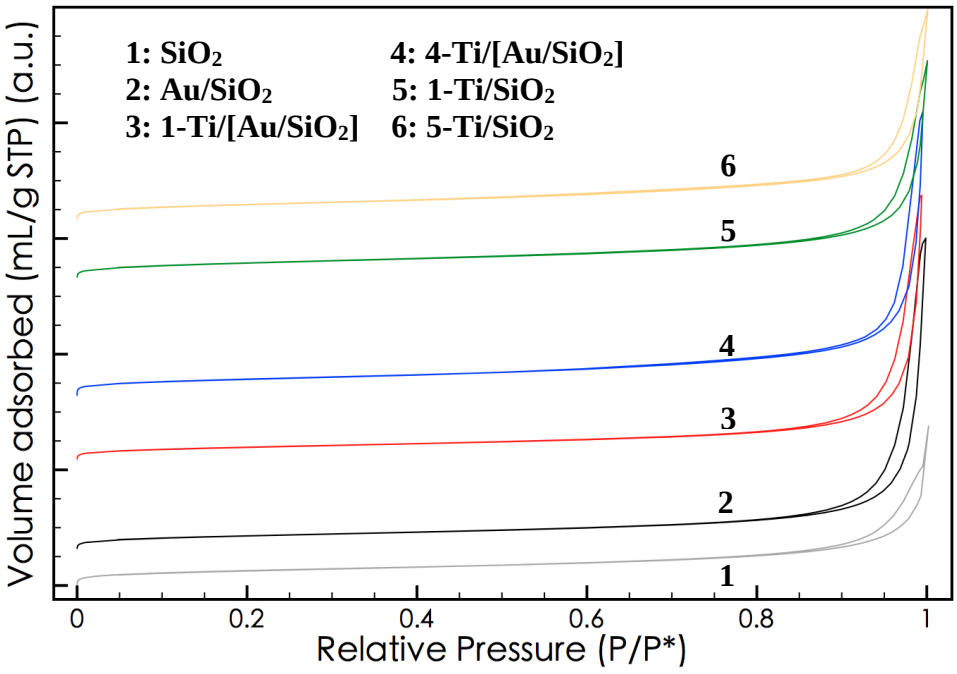

Figure 1. N_2 adsorption isotherms of catalysts. The isotherms are vertically displaced for clarity.

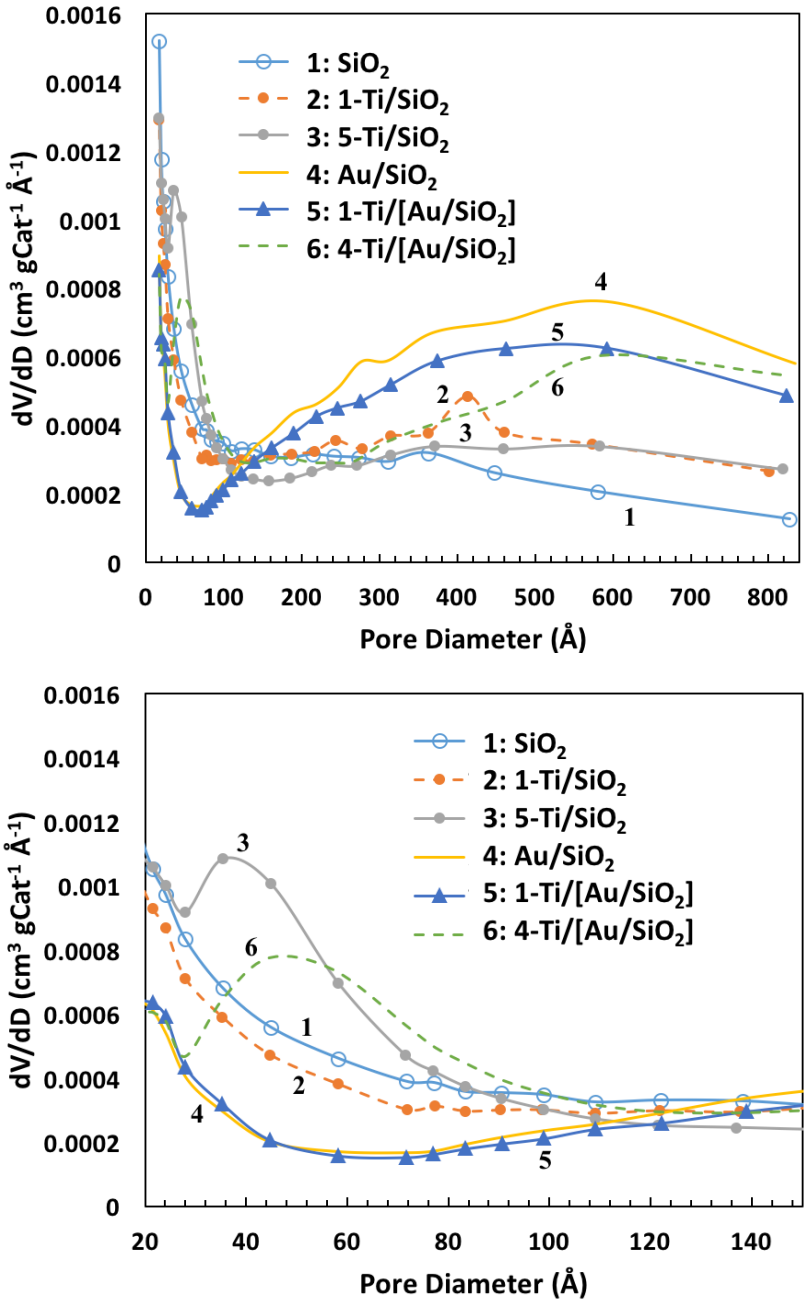

Figure 2. Barrett-Joyner-Halenda (BJH) pore size distributions. The bottom panel emphasizes the smaller diameter region.

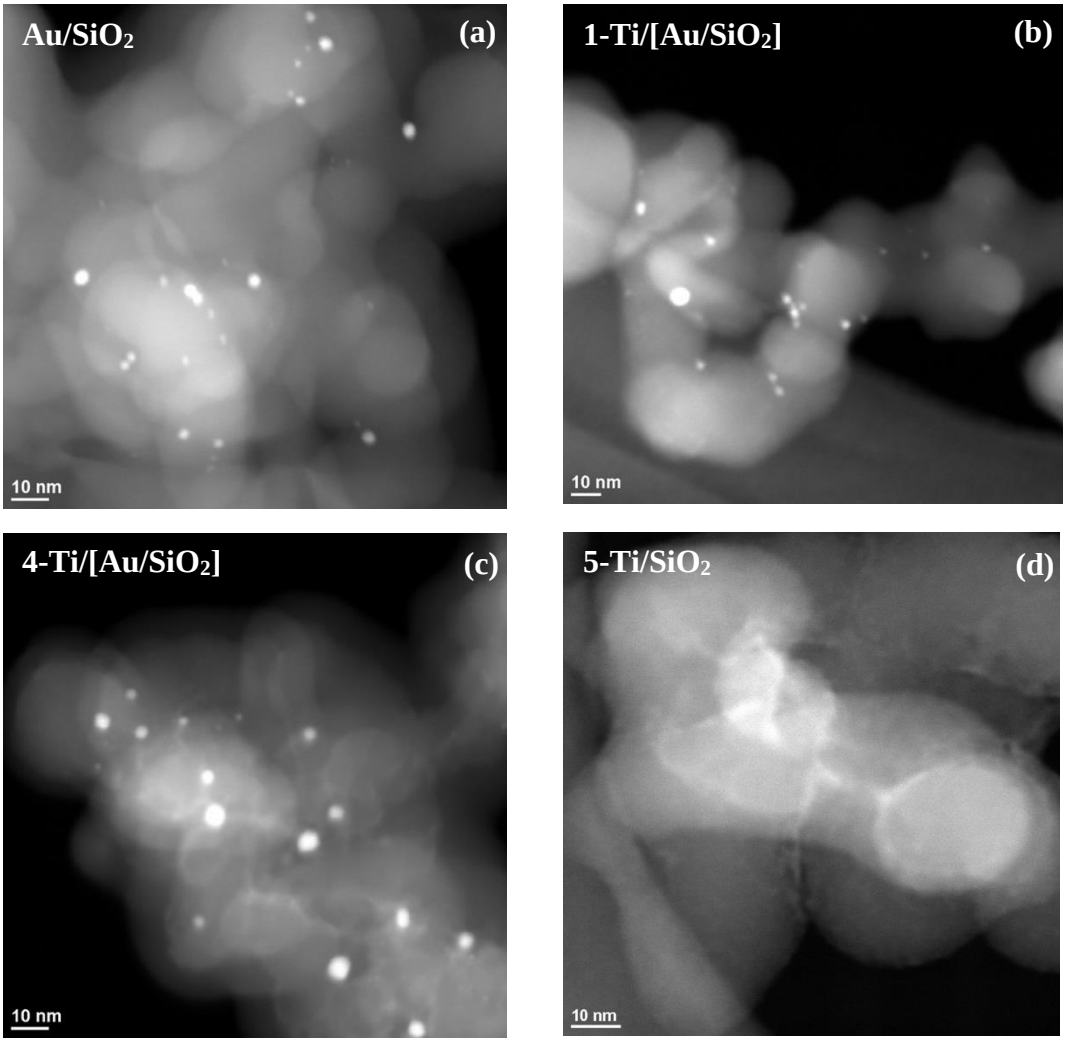

Figure 3. STEM images of (a) Au/SiO_2, (b) 1-Ti/[Au/SiO_2], (c) 4-Ti/[Au/SiO_2] and (d) 5-Ti/SiO_2 The STEM images were collected on catalysts after 2-propanol decomposition.

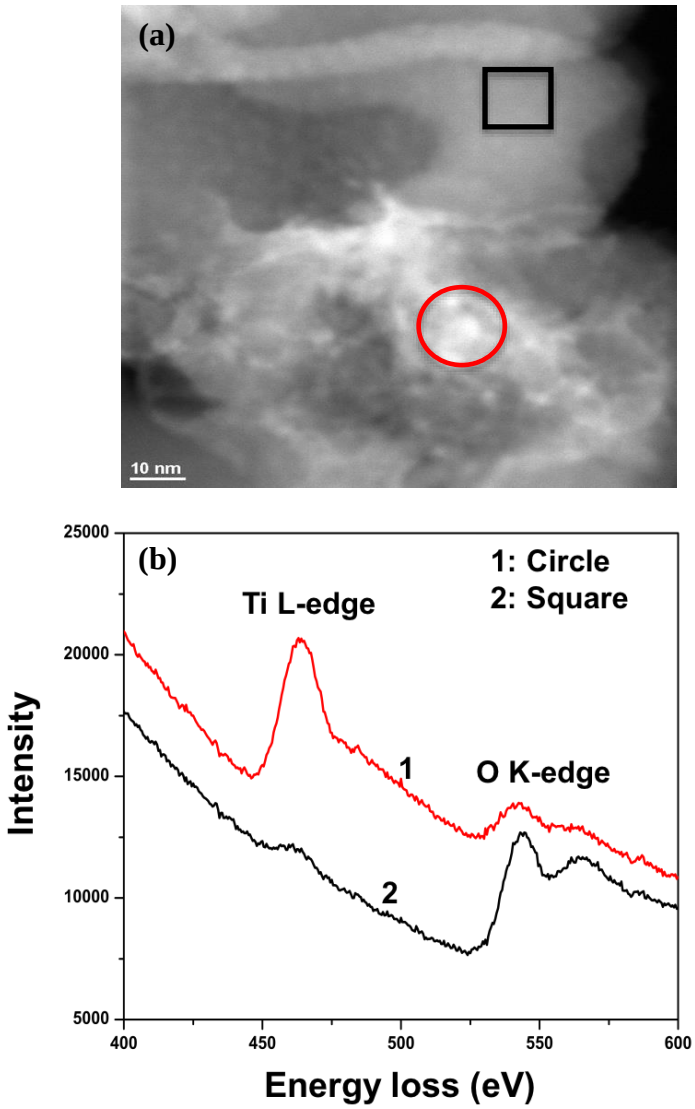

Figure 4. 5-Ti/SiO_2 after ozone treatment at 150 °C. (a) STEM image and (b) EELS spectra with the corresponding areas in the circle and square.

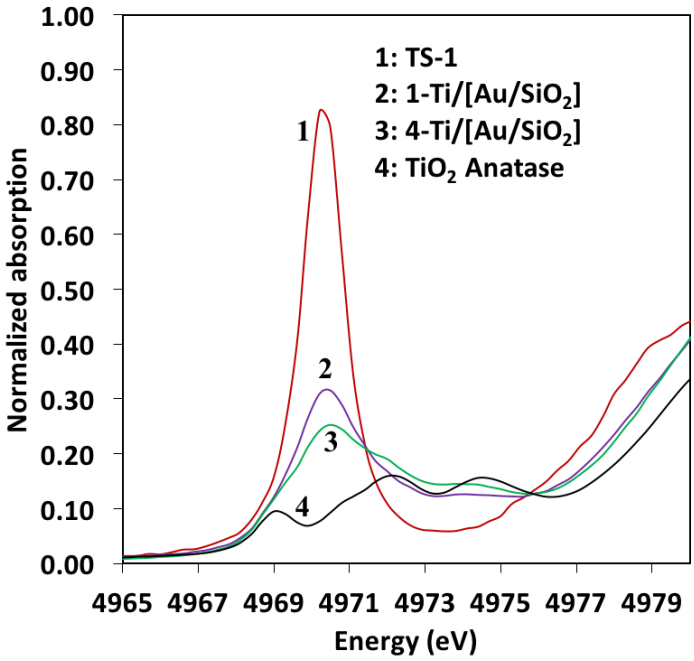

Figure 5. Pre-edge features of the Ti K-edge of the catalysts.

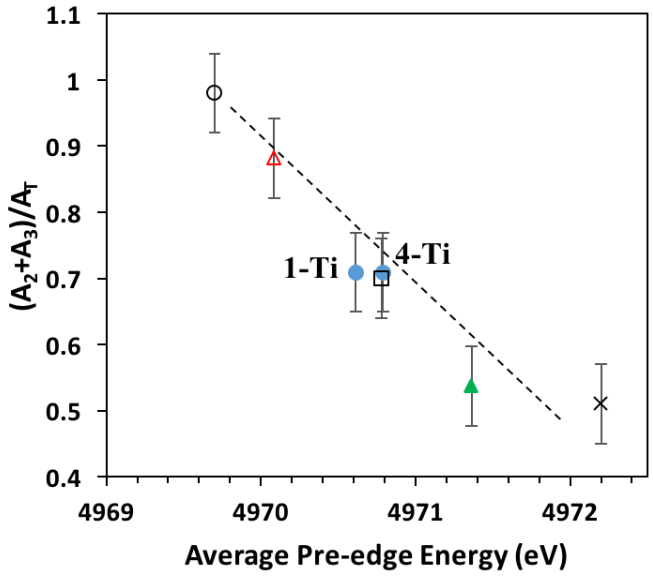

Figure 6. The relative area of peaks (A_2 + A_3)/A_T versus area-weighted average pre-edge energy, determined by the positions of A_2 and A_3. TS-1 (empty triangle), 1-Ti/[Au/SiO_2], 4-Ti/[Au/SiO_2] (solid circle) and anatase (solid triangle) in this study are plotted. Ba_2TiO_4 (empty circle), fresnoite (empty square) and anatase (cross) are taken from Todd et al.[29] A_T is the total area of pre-edge peaks (A_T=A_1 + A_2 + A_3 + A_B).

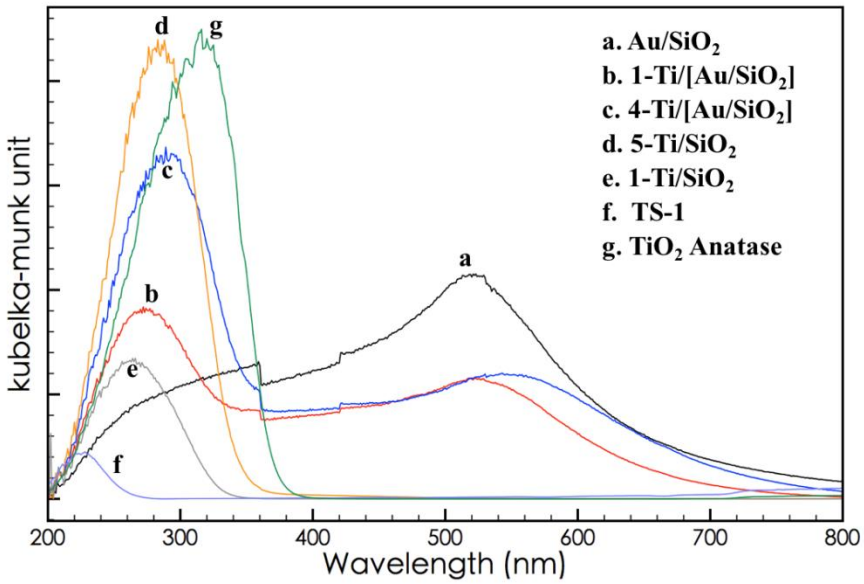

Figure 7. DR-UV-vis spectra of catalysts after reaction.

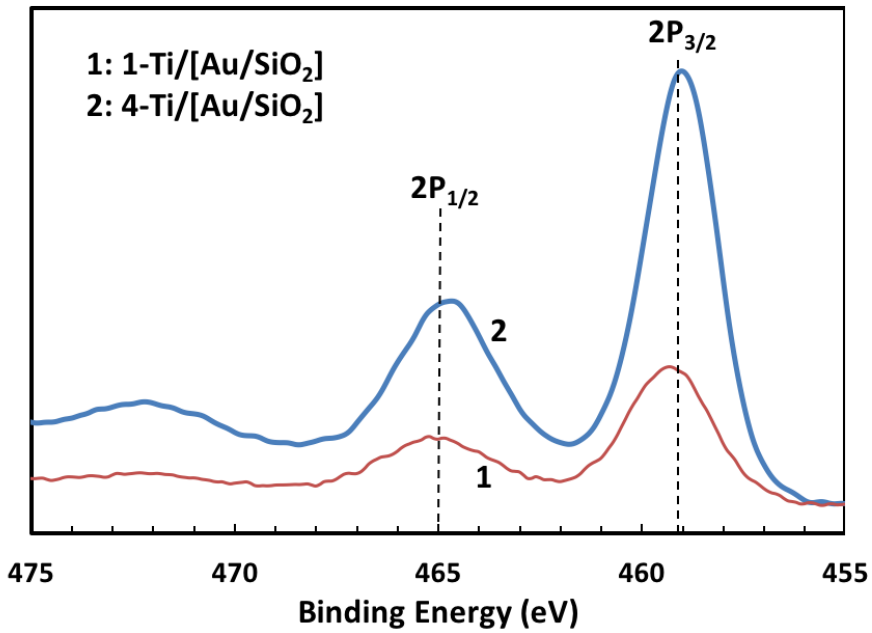

Figure 8. XPS of Ti 2p spectra for 1-Ti/[Au/SiO_2] and 4-Ti/[Au/SiO_2]. The samples had been treated with 300 cm^3 min^{-1} of 10% O_3/O_2 at 150 °C as part of the preparation procedure, and 50 cm^3 min^{-1} of 10% H_2/He at 180 °C for 1 h pretreatment before catalytic tests. They were exposed to air for XPS measurement.

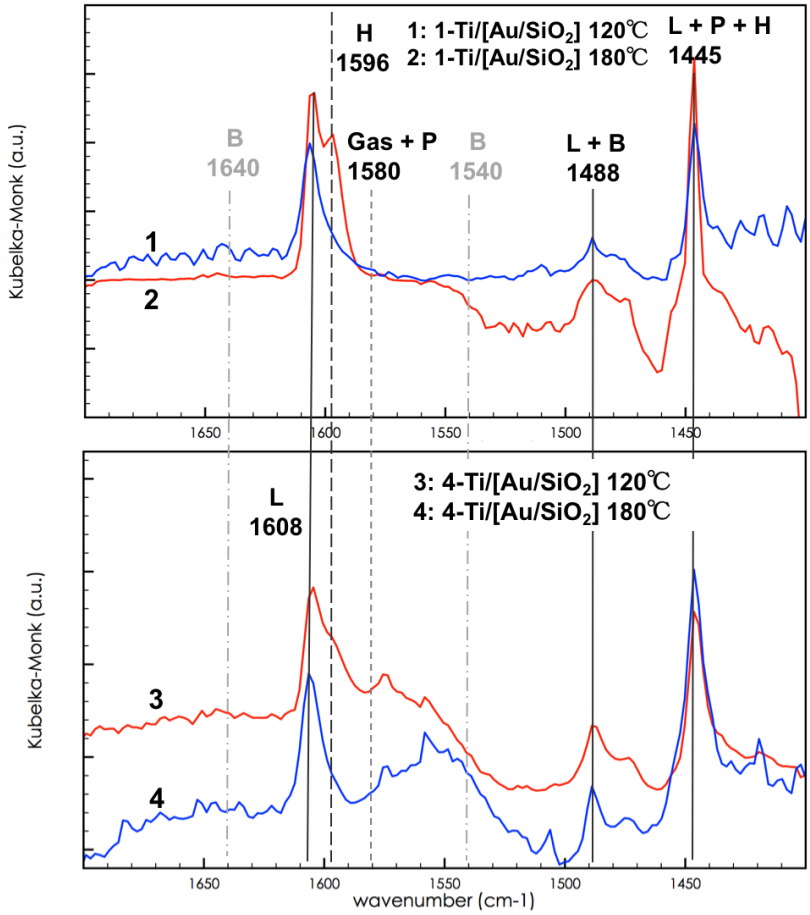

Figure 9. DRIFT spectra with pyridine adsorption on 1-Ti/[Au/SiO_2] and 4-Ti/[Au/SiO_2].

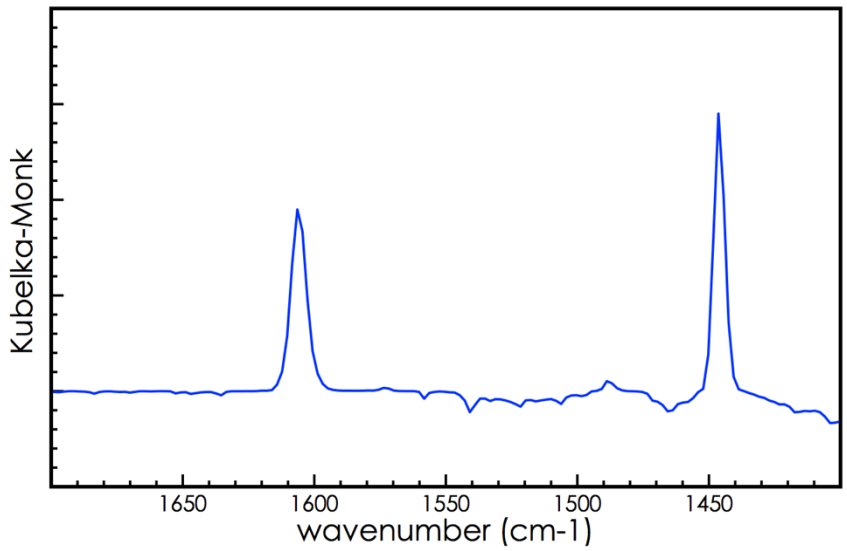

Figure 10. DRIFT spectra of 4-Ti/[Au/SiO_2] after adsorption of 2PrOH at 180 °C followed by exposure to pyridine at the same temperature. The spectrum was collected after He purging at 25 mL/min for 15 min.

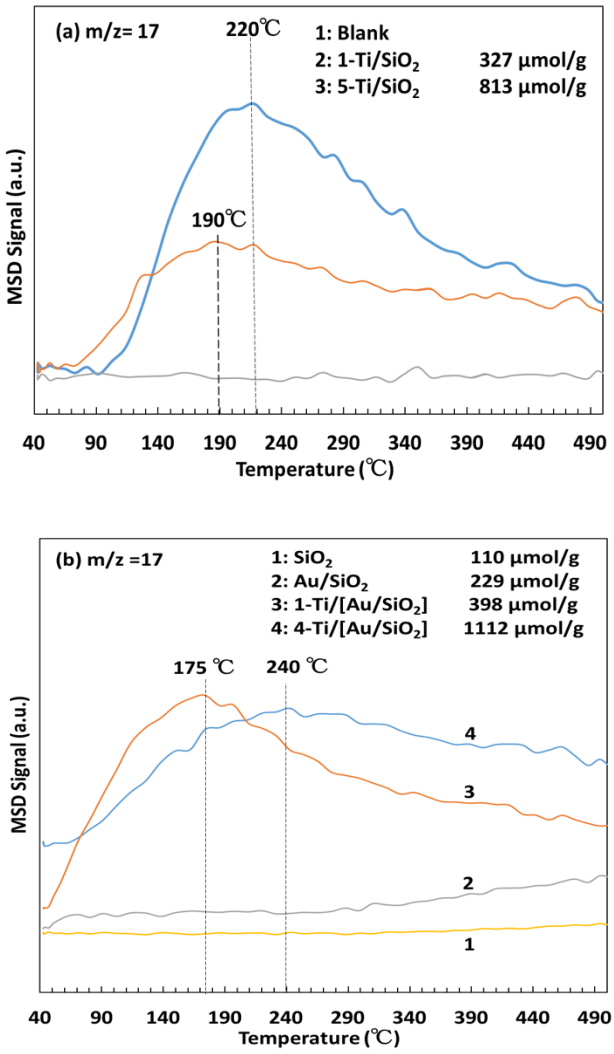

Figure 11. TPD-NH_3 spectra monitored with a mass spectrometer on (a) 1-Ti/SiO_2 and 5-Ti/SiO_2 (b) SiO_2, Au/SiO_2, 1-Ti[Au/SiO_2] and 4-Ti/[Au/SiO_2].

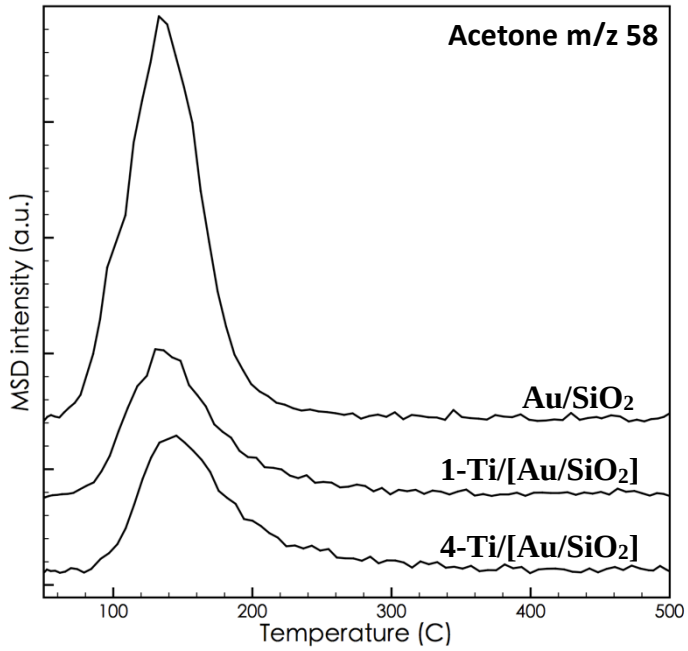

Figure 12. TPD of acetone on Au/SiO_2, 1-Ti/[Au/SiO_2] and 4-Ti/[Au/SiO_2].

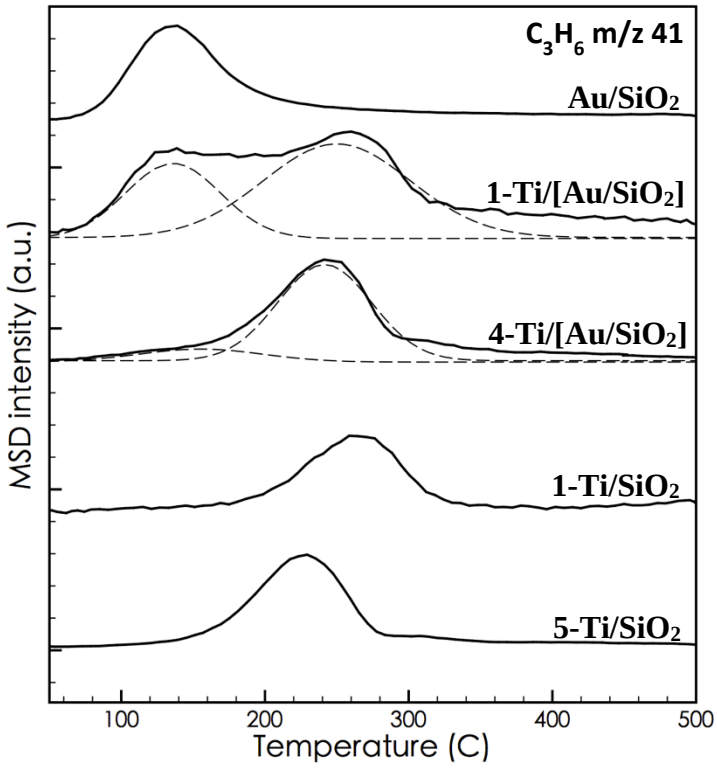

Figure 13. Propene evolution during TPRxn of 2-PrOH.

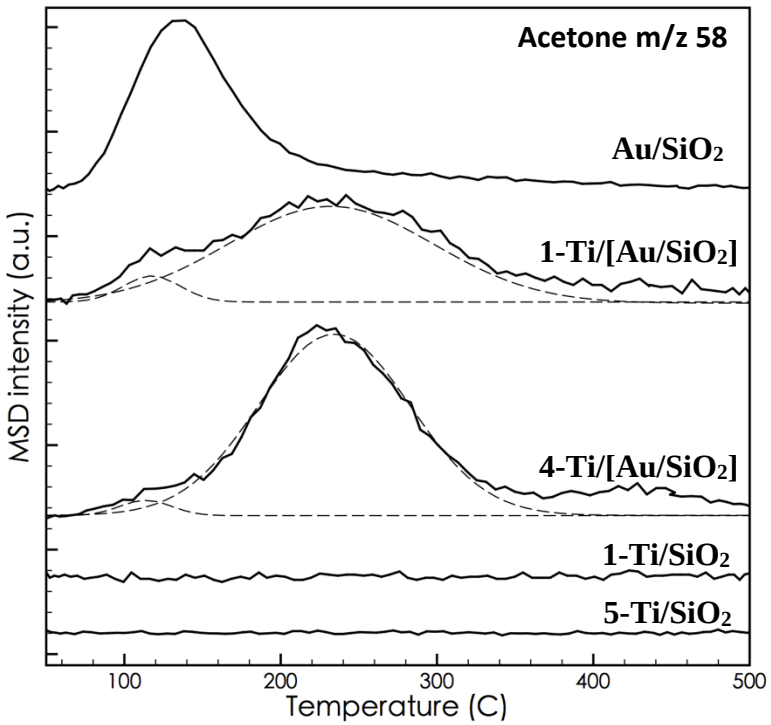

Figure 14. Acetone evolution during TPRxn of 2-propanol.

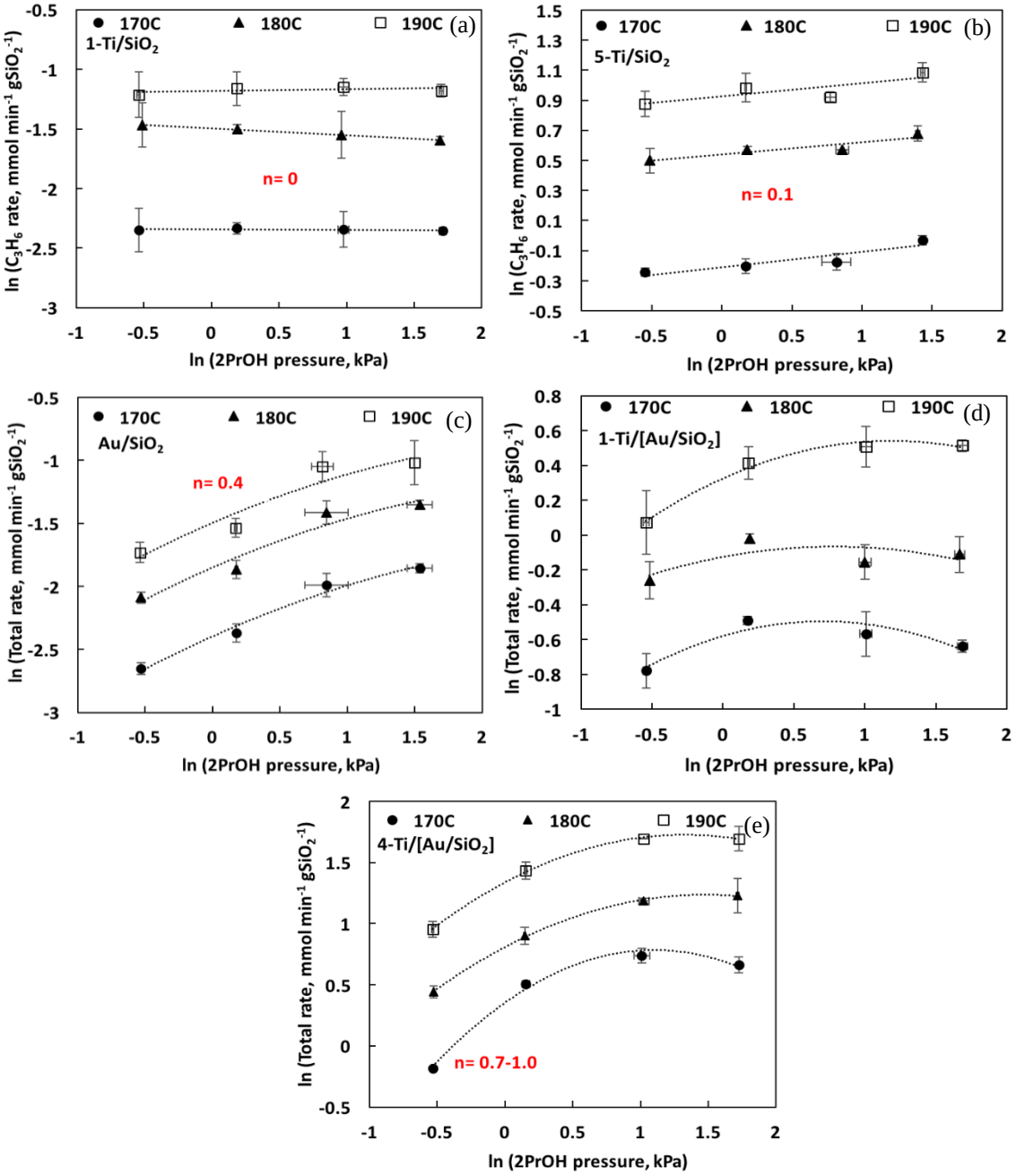

Figure 15. Dependence of 2-propanol decomposition rates on the partial pressure of 2-propanol on (a) 1-Ti/SiO_2, (b) 5-Ti/SiO_2, (c) Au/SiO_2, (d) 1-Ti/[Au/SiO_2], and (e) 4-Ti/[Au/SiO_2]. For both d and e, the rates shown are the observed rate minus the rates on Au/SiO_2. n is the reaction order obtained from the slopes.

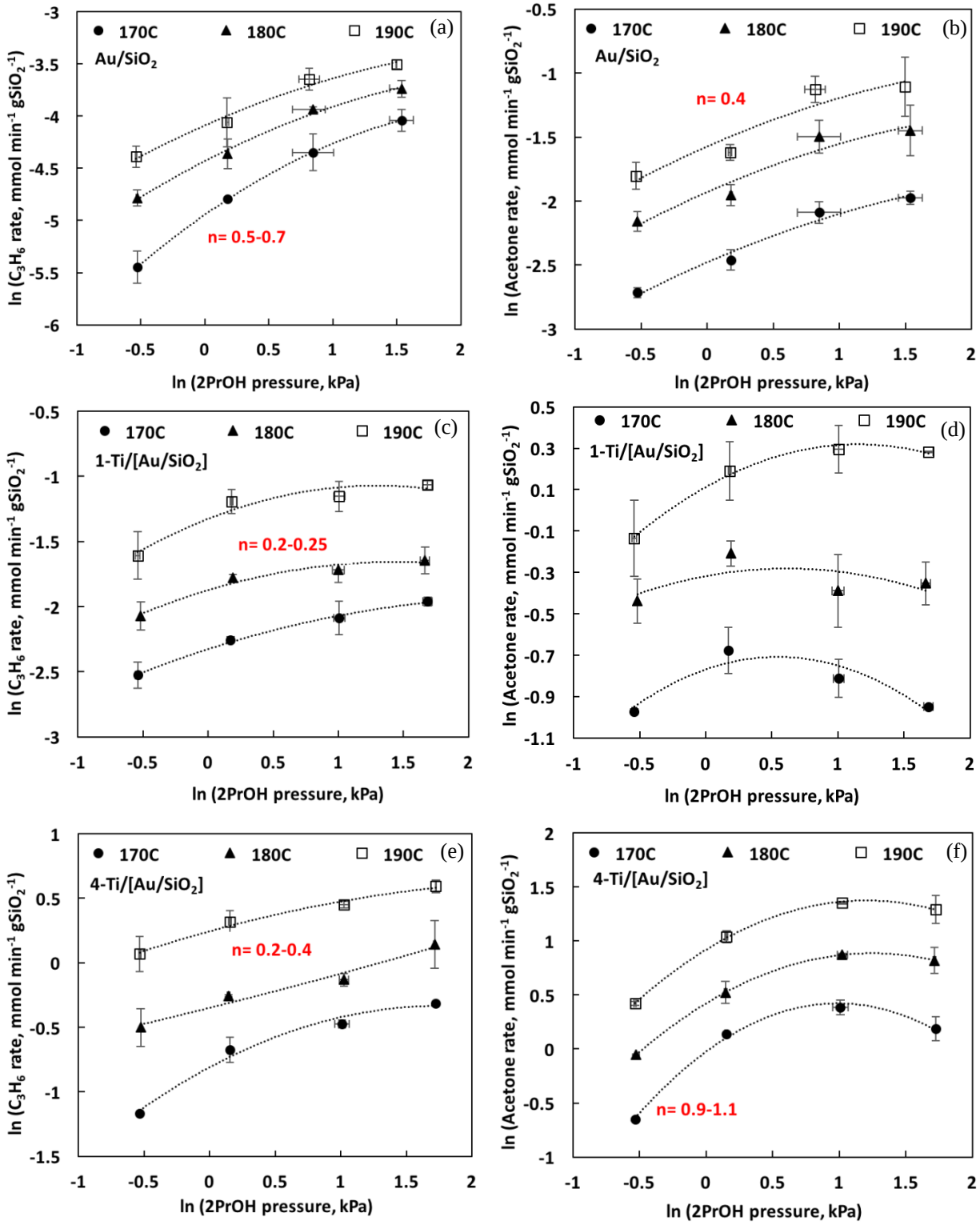

Figure 16. Dependence of propene (a, c, and e) and acetone (b, d, and f) production rates on the partial pressure of 2-propanol on (a, b) Au/SiO_2, (c, d) 1-Ti/[Au/SiO_2], and (e, f) 4-Ti/[Au/SiO_2].

For c, d, e, and f, the rates shown are the observed rate minus the rates on Au/SiO_2. n is the reaction order obtained from the slopes.

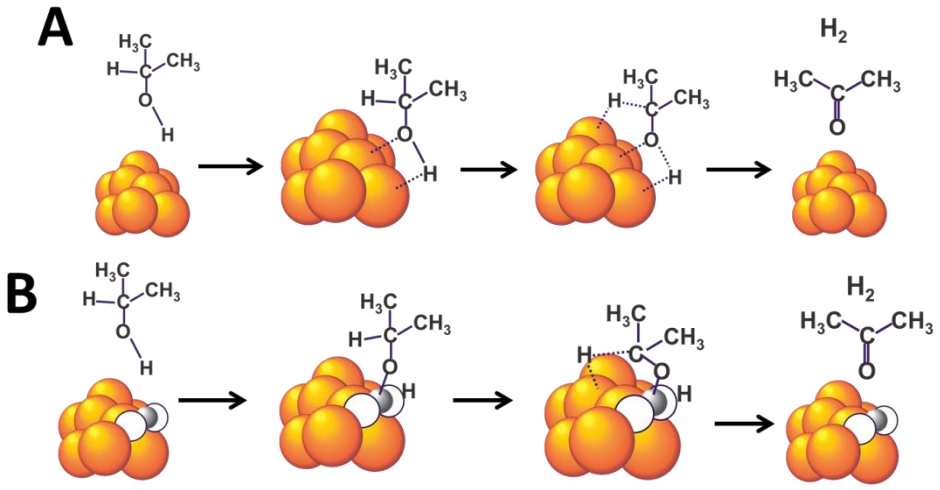

Figure 17. 2-propanol decomposition on (A) Au/SiO_2 and (B) $Ti/[Au/SiO_2]$.

Table 1. Compositions, Au particle sizes, and BET surface areas of the catalysts, based on weight of catalysts or weight of SiO_2.

Catalyst	Ti/Au (wt%)	S_{BET} (m^2 $gCat^{-1}$)[a]	S'_{BET} (m^2 $gSiO_2^{-1}$)[a]	D_p (nm)[b]
SiO_2	-	90	90	-
1-Ti/SiO_2	1.1/0	86	88	-
5-TiO_2/SiO_2	5.3/0	100	110	-
Au/SiO_2	0/1.1	92	93	1.6 ± 1.3
1-Ti/[Au/SiO_2]	0.8/1.1	83	85	1.8 ± 1.3
4-Ti/[Au/SiO_2]	4.1/1.1	109	118	1.7 ± 1.3

[a] S_{BET} is surface are based on one gram of catalyst, S'_{BET} is based on one gram of SiO_2.
[b] Au particle size determined by data from STEM images.

Table 2. EXAFS fitting parameters for Au catalysts after reaction

Sample	N_{Ti-O} (±20%)	R (Å) (±0.02Å)	N_{Au-Au} (±10%)	R (Å) (±0.005Å)	D_p (nm)
TS-1	4.0	1.80	-	-	-
Au/SiO_2	-	-	11.1	2.85	1.6 ± 1.3
1-Ti/[Au/SiO_2]	4.9	1.85	10.2	2.84	1.8 ± 1.3
4-Ti/[Au/SiO_2]	5.0	1.91	11.7	2.85	1.7 ± 1.3
Anatase	6.0	1.95	-	-	-
Au foil	-	-	12.0	2.86	-

Debye Waller factor and E_0 are summarized in Table S2.
(k^2: Δk=1.7-12.0 $Å^{-1}$ and Δr=1.0-2.0Å; S_0^2=0.96 for theoretical model of TiO_2 anatase).
(k^2: Δk=2.5-12.5 $Å^{-1}$ and Δr=2.0-3.3Å; S_0^2=0.86 for theoretical model of Au foil).

Table 3. The summary of DRIFTS results for pyridine adsorption

Catalyst	Temperature (°C)	LPy (cm^{-1})	HPy (cm^{-1})	PPy (cm^{-1})
SiO_2	28	-	1446,1598	1446,1580
1-Ti/SiO_2		1445,1488	1445,1596	1445,1582
5-Ti/SiO_2		1445,1488	1445,1596	1445,1582
Au/SiO_2		1446	1446,1598	1446,1580
1-Ti/[Au/SiO_2]		1445,1488	1445,1596	1445,1579
4-Ti/[Au/SiO_2]		1445,1488	1445,1596	1445,1580
SiO_2	120	-	1598	-
1-Ti/SiO_2		1447,1490,1608	1445,1596	-
5-Ti/SiO_2		1447,1488,1608	1445,1596	-
Au/SiO_2		-	1446,1598	-
1-Ti/[Au/SiO_2]		1445,1488,1608	1445,1596	-
4-Ti/[Au/SiO_2]		1445,1488,1608	1445,1596	-
SiO_2	180	-	-	-
1-Ti/SiO_2		1447,1608	-	-
5-Ti/SiO_2		1447,1488,1608	-	-
Au/SiO_2		-	1598	-
1-Ti/[Au/SiO_2]		1445,1488,1608	-	-
4-Ti/[Au/SiO_2]		1445,1488,1608	-	-

Table 4. Activation energies for TPD of acetone [a]

ν (min^{-1})	ln ν	$E_{a,\ des}$ (kJ/mol)
10^7	16.1	54.8
10^{11}	25.3	85.0
10^{12}	27.6	92.6

[a] Using the equation:

Table 5. The ratio of moles of acetone desorbed to surface Au in TPD of acetone

Catalyst	Catalyst weight (mg)	$Au_{surf.}$ [a] (μmol)	Acetone (μmol)	Acetone/$Au_{surf.}$
Au/SiO_2	89.7	2.5	9.5	3.8
1-Ti/[Au/SiO_2]	46.5	1.3	7.0	5.4
4-Ti/[Au/SiO_2]	31.8	0.9	5.0	5.6

[a] Surface dispersion ($1/D_p$) of 50% was used because the average Au particle size is ~2 nm for all the catalysts

Table 6. 2-propanol decomposition on supported Au catalysts[a]

Catalyst	Ti/Au (wt%)[b]	N_{acid} (μmol g^{-1})[c]	D_p (nm)[d]	Conv. (%)	Selectivity (%)		Rate (mmol min^{-1} $gSiO_2^{-1}$)	
					C_3H_6	Ace.	C_3H_6	Ace.
SiO_2	0/0	110	-	-	-	-	-	-
1-Ti/SiO_2	1.1/0	327	--	4.9	100	0	0.3±0.1	-
5-Ti/SiO_2	5.3/0	813	-	9.2	100	0	2.7±0.24	-
Au/SiO_2	0/1.1	229	1.6±1.3	4.6	8	92	0.02±0.01	0.2±0.1
1-Ti/[Au/SiO_2]	0.8/1.1	398	1.8±1.3	7.2	19	81	0.3±0.1	1.4±0.15
4-Ti/[Au/SiO_2]	4.1/1.1	1112	1.7±1.3	11.1	32	68	1.4±0.11	3.0±0.16
TiO_2[e]	0	NA	--	0.3	100	0	-	-
Au/TiO_2[e]	0.8	NA	2.8±3.2	32.0	1	99	-	-

[a] Reaction conditions: 2-PrOH=1.2 kPa, 30 cm^3 min^{-1}, 190 °C, 0.1 MPa, 2-2.5 h of reaction 25- 200 mg of catalyst. Ace. is acetone. NA means not available.
[b] Metal loadings were determined by ICP-OES
[c] The number of acid sites determined by TPD of NH_3, monitored with a TCD.
[d] Average Au nanoparticles were calculated by 200 counts with STEM images.
[e] 180 °C, 0.1 MPa, 60.5 mg of catalyst, 3-4.5 h of reaction, S_{BET} is 50 m^2 $gCat^{-1}$

Table 7. Preexponential factors A and activation energies E_a at partial pressures of 2-propanol when n=0

Catalyst	Total		Acetone		C_3H_6	
	ln A[a]	E_a (kJ mol^{-1})[a]	ln A[a]	E_a (kJ mol^{-1})[a]	ln A[a]	E_a (kJ mol^{-1})[a]
1-Ti/SiO_2[b]	24.9	100.1	-	-	24.9	100.1
5-Ti/SiO_2[b]	26.1	96.6	-	-	26.1	96.6
Au/SiO_2[c]	15.2	62.8	16.0	66.2	5[d]	33.1[d]
1-Ti/[Au/SiO_2][c]	26.0	98.1	27.5	105.0	18.6	76.0
4-Ti/[Au/SiO_2][c]	24.6	88.2	25.8	94.2	20.6	77.2

[a]The uncertainties in E_a and ln A are 5%.
[b]Average values at the four partial pressures of 2-propanol
[c] At 5.6 kPa (ln P= 1.7)
[d] Because of the small amounts of propene formed, the uncertainties in these numbers were high.

Table 8. Catalytic results of 2-propanol oxidation with O_2

Catalyst	Ti/Au (wt%)[a]	D_p (nm)[b]	Conv. (%)	Selectivity (%)	
				C_3H_6	Acetone
1-Ti/SiO_2	1.1/0	--	0.4	100	0
5-Ti/SiO_2	5.3/0	-	2.1	100	0
Au/SiO_2	0/1.1	1.6±1.3	39.7	0	100
1-Ti/[Au/SiO_2]	0.8/1.1	1.8±1.3	21.3	2	98
4-Ti/[Au/SiO_2]	4.1/1.1	1.7±1.3	12.5	6	94

2-PrOH/O_2/He=1.2/5/93.8, 30 mL min^{-1}, 180 °C